ENHANCEMENT OF SEASAT WIND-STRESS MEASUREMENTS

USING DATA FROM GOES

A REPORT
from the space science and engineering center
the university of wisconsin-madison
madison, wisconsin

ENHANCEMENT OF SEASAT WIND-STRESS MEASUREMENTS

USING DATA FROM GOES

FINAL REPORT

August 1983

Final Report to

U.S. DEPARTMENT OF Commerce
NATIONAL OCEANIC AND ATMOSPHERIC ADMINISTRATION

for

Enhancement of SEASAT Wind-Stress Measurements
Using Data from GOES

For the Period of

1 October 1978 to 31 December 1981

Verner E. Suomi, Principal Investigator

Submitted by

Barry B. Hinton and Donald P. Wylie

Space Science and Engineering Center
at the University of Wisconsin-Madison
1225 West Dayton Street
Madison, Wisconsin 53706
(608) 262-0544

August 1983

TABLE OF CONTENTS

List of Tables

Figures

Fig. 1.   SEASAT scatterometer surface winds. Aliases supplied by the
           geophysical data record algorithms are shown.

Fig. 2.   The vertical distributions of cloud tops for 9 July 1979.

Fig. 3.   Alias removal.

Fig. 4.   Correlation between pairs of observations as a function of
           spatial separation.

Fig. 5.   Scatterometer directional skill. This figure shows the relative
           frequency with which the alias selected with the help of cloud
           motions corresponded to the probability rank of the alias in the
           interim geophysical data record for a 7-degree of arc long
           segment of pars 1339. Some segments show higher skill -- usually
           when only two aliases are presented.

Fig. 6.   Estimates of the vertical resolution of satellite-derived
           temperature profiles by the Twomey method. Curves indicate vertical
           averaging for estimating temperatures at discrete pressure levels as
           noted by numbers at each peak.

Fig. 7.   Key to the boxes listed in Table 5.

Fig. 8.   Relations between speed and dispersion of the veering angle, and
           between steadiness and dispersion of the veering angle for the
           area shown in Fig. 7 during January, February, June, July, and
           August 1979.

Fig. 9.   Relation between speed and steadiness. The data cover the same
           spatial region and time period as Figure 8.

Fig. 10.   Growth of directional differences between pairs ship wind
           observations with increasing separation between the ships. One
           degree of arc is about 110 km. The data come from the region
           shown in Fig. 7.

Fig. 11.   A GOES-East image of the North Atlantic on 1700 GMT
           17 September 1978.

Fig. 12.   A composite surface air temperature analysis for the North
           Atlantic made from all ship reports from 00 GMT 14 September to
           1200 GMT 17 September 1978. The track of tropical storm Hope
           from 13 September to 17 September is indicated by the bold line.

Fig. 13.   A composite surface ocean temperature analysis for the North
           Atlantic made from all ship reports from 00 GMT 14 September to
           1200 GMT 17 September 1978. The arrows depict the northern
           boundary of the Gulf Stream from the NOAA/NESS Gulf Stream
           analysis 17-20 September 1978.

1. Introduction

   This report summarizes work done at the Space Science and Engineering Center from 1 October 1978 to 30 December 1981 to study the relationships of low level cloud motions to near surface winds over the oceans, and in particular the near surface winds measured by the active microwave scatterometer on SEASAT-A. Our approach to this work was largely empirical, with theoretical guidance only. Consequently, this report largely discusses comparisons of data, and simple methods of handling the data.

   The purpose of this work was to develop a practical technique to remove the directional ambiguity of the scatterometer winds recovered by the processing algorithms for the geophysical data records (see Fig. 1). This technique could then be used to "de-alias" the data and produce uniquely defined wind fields. Presumably, the technique could also be incorporated directly into the processing stream for an operational scatterometer of the SEASAT type.

   Specifically, this report discusses the relationship of winds at cloud level with mast level winds as observed by island-based radiosonde stations, cloud motions, sun glint, and ships as well as SEASAT. We are particularly interested in the veering, or rotation of the direction of the wind with height, geographical variations of its mean value, and the dispersion or standard deviation of the veering about the mean. The latter is the most critical parameter. As long as it is of the order of 45° or less, the alias removal technique should be workable. Another property that must be considered is the horizontal variation of the wind direction over the oceans. It largely determines how many clouds must be tracked, or over how large a portion of a SEASAT swath each cloud motion may be used to
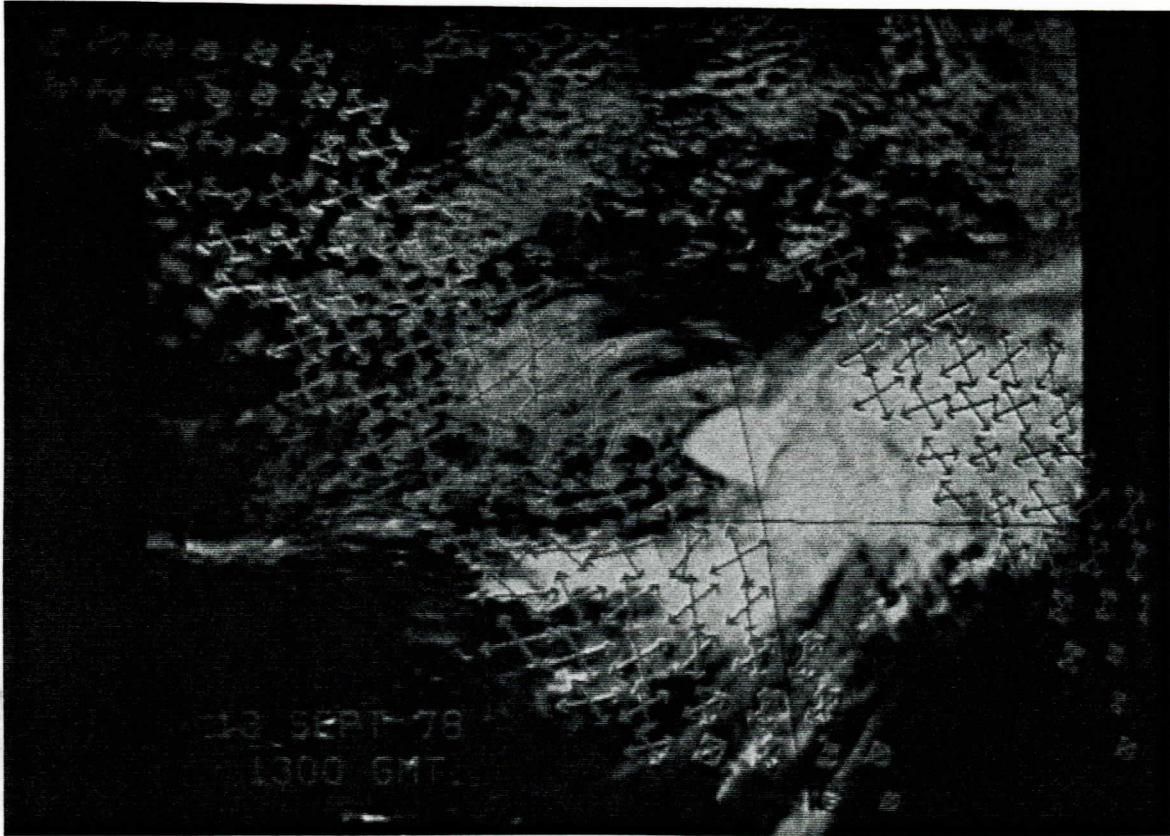
Fig. 1. SEASAT scatterometer surface winds. Aliases supplied by the geophysical data record algorithms are shown.

select the best alias vector from those available. Further, we shall mention results of some subsidiary investigations into the quality of the "truth data". Finally, we discuss the future outlook for scatterometry with respect to the alias problem.

2. Background

2.1 Cloud Motions

For the sake of readers unfamiliar with either the scatterometer or winds determined from cloud motions, we will briefly discuss them and give references to further information.

The United States GOES satellites normally occupy two stations in geostationary orbits. GOES-E is about 37,000 km above 0°N, 75°E and GOES-W is about 37,000 km above 0°N, 135°E. During routine operation, each spacecraft scans the earth once each half-hour and forms an image in a visible band centered at 0.605 microns and a thermal infrared band at about 11 microns. The images are composed of digitally recorded samples (pixels) whose size varies with distance from the subsatellite point. Maximum resolution is just under 1 km for the visible image and about 8 km for the infrared. The orbits are well behaved so that the orbital parameters obtained from tracking data (with small corrections obtained from landmark measurements) can be used to precisely locate each pixel. Thus, by locating a cloud feature in a series of images, its displacement in 30-minute time increments can be determined. More general descriptions have been given by Mosher (1979) and Hubert (1979).

Specifically, we display a representative portion of each of three or more satellite images displayed on a television frame which is coupled to our interactive data analysis system, McIDAS (Suomi et al., 1983). These frames are looped to present an animated "movie" of the cloud motions. An

3

analyst selects a suitable cloud by placing a joystick-driven box over it -- usually after the display has been stopped and frozen on the first frame. He then slowly steps through the sequence, keeping the cloud within the box. It is not necessary to precisely align the cursor; the displacement is determined by a correlation method in which the best fit of the cloud image at the second time to the image at the first time is used as the criterion. Quality control procedures are invoked and the wind is discarded if the wind measured from t_2 to t_3 varies too greatly from the t_1 to t_2 wind, or if the correlation peak is on the edge of the cursor box.

Selection of a suitable cloud is a critical step. Because they more accurately reflect surface wind, very small, low-level, short-lived clouds are desirable. On the other hand, very small clouds can only be located to within a pixel. Larger clouds, having more than one identifiable feature, can be located by the correlation algorithm to within a fraction of a pixel (of the order of $1/n^{\frac{1}{2}}$, where n is the number of distinctly identifiable features). Also, if the clouds are both small and too short-lived, false tracking may result from matching a single pixel cloud, which disappears and is absent from a subsequent image, with a new single pixel cloud which forms nearby. To avoid false targets, one can track more clouds than would otherwise be required and demand consistency with nearby cloud motions in an editing process. In some cases, the small clouds will be dense enough to allow a group of them to be contained within the allowable sizes of cursor boxes and tracked as a group. In effect this is much like tracking a larger complex cloud. A quantitative estimate of the height of cloud top is available from the IR, and can often be discerned from the appearance of the clouds in the visible.

4

2.2 Scatterometer Observations

The equipment constituting the SEASAT scatterometer is described by Grantham et al. (1977) and by Johnson et al. (1980), along with the principles of operation. (See also Grantham et al., 1982.) For descriptive purposes, the scatterometer is sometimes compared to the studies of Cox and Munk (1954) in which the scattering of visible light from the sun by the sea is related to the distribution of slopes produced by the action of wind roughening the water surface. However, the Cox and Munk treatment is founded on the limiting case of geometrical optics. As is mentioned in the references cited, geometrical optics are not adequate in the microwave scatterometer case. The surface deformation usually has prominent components at spatial wave numbers the same orders as the scatterometer wave number. Hence, microwave scattering off the sea surface arises from Bragg scattering from these short waves mixed with the effects of tilting the surface by longer gravity waves and swell, which is essentially a geometrical optics effect. The radar backscatter could be calculated from first principles for a known surface shape, using the dielectric properties of sea water. However, the ultimate application is to know the surface stress, or the low level wind, and it is not possible at present to relate these to specific surface shapes so that one must resort to empirical studies.

3. Research Investigations for Alias Removal

3.1 Relation of Cloud Motions to Surface Winds

This research commenced before scatterometer data were available. Consequently, we first investigated observed relationships between low

level winds with cloud motions, and the properties of low level wind profiles over the oceans.

The terminology used in this report is not completely standardized, and requires explanation. We use "veering" to denote differences in direction of the wind. The direction of the wind denotes the compass point from which the wind is blowing; that is, a wind direction of 90° signifies a wind blowing from the east toward the west. The magnitude and sense of the veering with increasing height, a, are defined by (1) in which θ is the wind direction and Z altitude.

$$a = \theta(Z_2) - \theta(Z_1) \quad \text{for } Z_2 \geq Z_1 \tag{1}$$

Thus, positive veering with height indicates a clockwise rotation of the wind vector with increasing altitude in either hemisphere and must not be confused with a cyclonic or anticyclonic rotation with height.

We obtained a set of rawinsonde observations for summer and autumn 1978 from real-time reports derived from the Global Telecommunications System and carried on the WB604 communications line. Of the stations available on this circuit, Swan Island, Bermuda, St. Paul Island, and Ocean Station-P (see Table 1 for station locations) were deemed to be representative of marine conditions. Consideration was given to distance from a continental barrier, size of island, and altitude.

Here we shall cite what we believe to be the salient results from this study. Table 2 summarizes the results for veering between the surface and the 850 mb level from the four stations. Table 3 gives the equivalent results in terms of the zonal (u) component and meridional (v) component of the wind. Mean and standard deviation values are shown in the form, XX±XX. Dispersion denotes the rms error which would result if linear regression

6

Table 1. Station Locations

Name	Latitude (deg.)	Longitude (deg.)	ID Number
St. Paul Island	57 N	170 W	70308
Swan Island	17 N	84 W	78501
Station-P	50 N	145 W	99021
Bermuda	32 N	65 W	78016

Table 2. Veering between the surface and the 850 mb level. Dispersion is the root mean square deviation of a predicted surface parameter (obtained by a regression equation from the 850 mb value) from the observed surface value. S.D. denotes standard deviation, or root mean square deviation from the mean.

STATION	SAMPLES Number (n)	PRESSURE LEVEL p (mb)	REPORTED DIRECTION (Θ)			VEERING ($\alpha=\Theta(Z)-\Theta(sfc)$)		
			Mean±S.D. (deg)	Dispersion (deg)	Correlation to sfc value*	Mean±S.D. (deg)	Dispersion (deg)	Correlation w. sfc Θ**
78016 Bermuda	112 112	0 850	205±99 192±103	34	.94	12.9±34	33	-.27
99021 OWS-P	79 79	0 850	256±69 240±78	35	.90	15.9±35	31	-.48
70308 St. Paul	100 100	0 850	182±104 170±107	26	.97	12.1±26	25	-.23
78501 Swan Is.	123 123	0 850	122±86 107±86	34	.92	13.9±35	35	-.19

* This column shows the correlation of the direction reported for 850 mb to the direction reported at the surface.

** This column shows the correlation of the directional difference between the 850 mb level and the surface with the surface direction. In other words, it shows the relation of the veering to the surface direction, and allows us to conclude that, except at OWS-P, the veering does not depend too much on wind direction.

Table 3. Relation of wind and streamline components of the surface to those at the 850 mb level. Dispersion is the root mean square deviation from the prediction (based on a regression equation) of surface values by 850 mb values. S.D. denotes standard deviation or root mean square deviation from the mean.

STATION	SAMPLES Number (n)	ALTITUDE (mb)	ZONAL COMPONENT (u) Mean±S.D. (ms⁻¹)	Dispersion S.D. (ms⁻¹)	Correlation	MERIDIONAL COMPONENT (v) Mean±S.D. (ms⁻¹)	Dispersion S.D. (ms⁻¹)	Correlation	ZONAL STREAMLINE COMP. −sinθ	Dispersion of sinθ	Corr. r(sinθ)	MERIDIONAL STREAMLINE COMP. −cosθ	Dispersion of cosθ	Corr. r(cosθ)
78016	112	0	1.36±4.6			−0.71±5.5			.09±.72			−.01±.69		
	112	850	6.44±6.7	2.8	.87	−0.39±11.2	2.5	.84	.28±.72	.37	.86	.00±.64	.40	.86
99021	79	0	4.66±6.4			−1.27±6.5			.43±.64			−.08±.63		
	79	850	7.52±7.6	3.5	.85	−0.52±7.5	3.8	.81	.60±.57	.42	.75	.01±.57	.37	.82
70308	100	0	−1.33±6.0			0.39±7.4			−.13±.68			.01±.73		
	100	850	−0.91±9.1	2.6	.90	−1.55±10.6	2.8	.93	−.03±.70	.33	.87	−.06±.72	.30	.91
78501	123	0	−3.29±2.4			0.71±3.3			−.69±.43			.21±.55		
	123	850	−5.08±4.1	2.0	.56	−0.38±3.7	2.6	.61	−.67±.48	.33	.65	.01±.56	.39	.71

equations derived from this data set were used to predict surface values from 850 mb values.

The mean veering between these levels does not differ greatly among the stations, the dispersions are all under 36°, and, as far as one can determine from the given sample, the veering is essentially independent of the surface direction. Moreover, the 850 mb direction has significant skill for predicting the surface direction. In every case, the dispersion is less than half the variance of the surface wind. Evidently, an 850 mb wind could resolve scatterometer ambiguities unless two or more aliases were within 40° of the predicted wind direction.

Low level clouds over the oceans reflect air motion near their bases which are usually somewhat below the height of the 850 mb pressure level, typically 900 to 925 mb. Fig. 2 shows the mean pressure altitude of the tops of low clouds about 870 mb. Thus, the 850 mb results are conservative. However, in the event the height varies, or it is necessary to combine data from various heights in an analysis, it is useful to know how winds at altitude vary from surface winds as the altitude varies.

For two stations, St. Paul (70308) and Swan Island (78502), significant level wind data were routinely transmitted in real time. We were surprised to note that at both stations there was considerable skill in inferring surface wind direction at altitudes at least up to 1829 m, which is well above the 850 mb level. These results are summarized in Table 4. Incidentally, we note that Table 4 shows that there is skill in predicting surface speed at St. Paul, but very little at Swan Island.

While all the above results for a few specific locations can hardly be extrapolated to a global generality, they are indicative and justify the
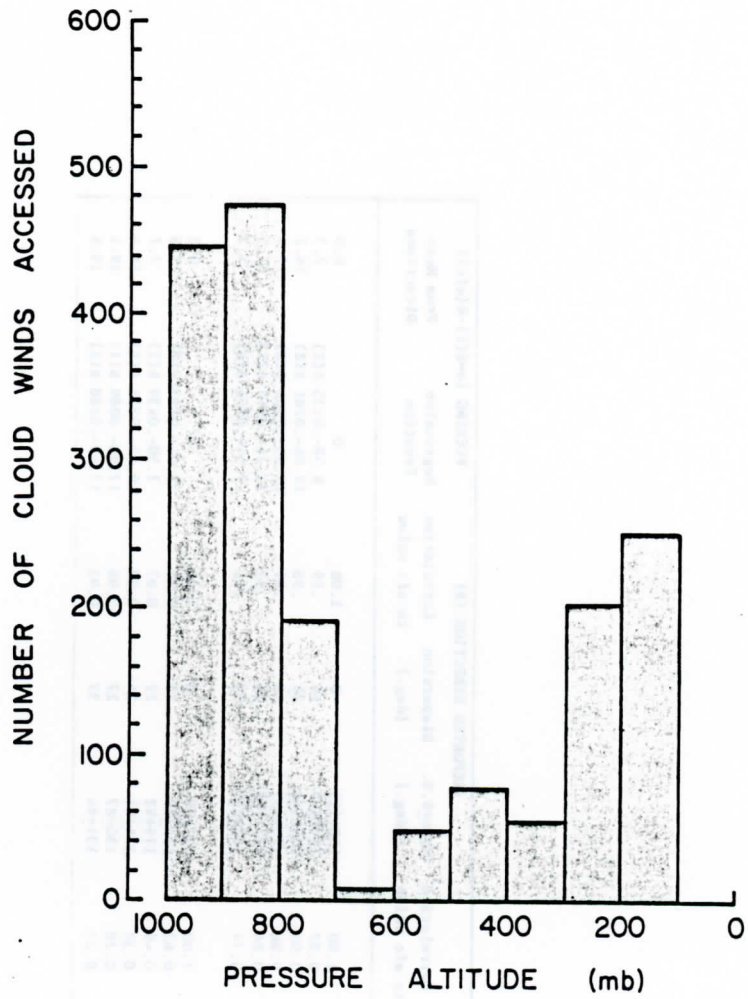
Fig. 2.   The vertical distributions of cloud tops for 9 July 1979.

Table 4. Velocity data for St. Paul Island and Swan Island. The columns labeled dispersion indicate the rms deviation of the value predicted by a linear regression equation of the form a + bz from actual data values. Therefore, dispersion is representative of the errors we would make in an estimate of speed or direction. S.D. (standard deviation) refers to the rms deviation from the sample mean. When dispersion is significantly less than the variance, the estimate shows skill. The final column on the right is the veering calculated from the regression equation, using the mean value of the direction, and is intended to represent a typical or characteristic value of veering.

STATION	SAMPLES Number (n)	ALTITUDE z (m)	SPEED (V) Mean±S.D. (ms⁻¹)	Dispersion (ms⁻¹)	Correlation to sfc value	REPORTED DIRECTION (θ) Mean±S.D. (deg.)	Dispersion (deg.)	Correlation to sfc value	VEERING (α=θ(Z)-θ(sfc)) Regression Equation	From Mean Directions
70308	43	0	9.4±5.0	0-	1.00	159±115	0	1.00	0	0.0
		304	12.1±6.7	2.5	0.87	167±112	14	.99	9.58-.0135 θ(Z)	7.3
		609	11.9±7.0	2.2	0.90	173±109	25	.98	19.06-.0281 θ(Z)	14.2
		914	11.7±7.2	2.6	0.86	173±107	28	.97	19.93-.0366 θ(Z)	13.6
		1219	11.7±7.6	2.8	0.84	171±104	26	.97	23.76-.0717 θ(Z)	11.5
		1829	11.6±7.8	3.1	0.79	165±119	35	.95	-7.54+.0776 θ(Z)	5.3
78501	52	0	5.6±2.5	0	1.00	111±90	0	1.00	0	0.0
		304	7.4±2.3	2.0	0.62	114±90	18	0.98	2.01-.0153 θ(Z)	3.8
		609	7.7±2.6	2.2	0.49	119±92	22	0.97	2.50-.0439 θ(Z)	7.7
		914	7.3±2.9	2.3	0.38	126±91	24	0.97	10.43-.0371 θ(Z)	18.1
		1219	7.1±3.0	2.4	0.28	130±87	27	0.96	17.90-.0089 θ(Z)	19.1
		1829	7.0±3.1	3.1	0.22	131±84	37	0.91	17.19-.0188 θ(Z)	19.6

use of low level cloud motions -- at least in some areas. We will return to this problem later.

3.2 Comparison of Cloud Motions, Sun glint, and Scatterometer Winds

As soon as SEASAT data were available, we undertook a small-scale validation study in which surface wind estimates from cloud motions, from an adaptation of the Cox and Munk method to GOES images, and from the scatterometer were compared (Wylie et al., 1981; see Appendix A). As a part of this research, we used cloud motions to select the best alias from the scatterometer. For present purposes, the principal results were that for the very small number of cases (7) for which the surface wind directions were available from nearby ships, the scatter of the selected SEASAT directions about the ship direction was 13°. Similarly, for ships compared directly with cloud motions, the scatter was 22°.

3.3 Alias Removal Methods

Our earliest semi-automated alias selection method consisted of the following steps: First, an appropriate set of images from GOES-E or GOES-W was displayed to match the time and location of the scatterometer data swath and the scatterometer data read into McIDAS. The scatterometer winds (all aliases) were then plotted as a graphic overlay on the images. Using this overlay to define the area of principal interest, suitable clouds were selected and tracked by the McIDAS WINDCO software to obtain cloud motion vectors in sufficient numbers and distributed so as to define the principal flow features (i.e., centers of circulation, cols confluences, etc.). These vectors were also overlaid on the image -- either in wider lines or a different color for clarity. Next, the cursor was moved by joysticks to overlay as many groups of aliases as desired by expanding its size and controlling its shape by means of a second joystick. A keyboard command

13

was then entered to edit the aliases, "blowing away" or flagging the unwanted ones in the file. The process is illustrated in Fig. 3.

In order to further develop our algorithm removal scheme, and to provide for eventual automation, it was necessary to quantitatively consider the horizontal scale of wind variations. One cannot generate a cloud motion vector directly over each scatterometer observation. However, for each set of ambiguities, a directional determination is required. How close must it be? This question is answered by closely related research carried out for another program (Wylie and Hinton, 1981). The salient results are shown in Fig. 4. Among other things, this shows that objective analyses of cloud motions, incorporating two to ten observations per grid point on a 1° by 1° to 4° by 4° latitude-longitude grid combined with the weighting function, Wt, given by (2) with D =2, C = 6, would correlate well with ship observations near a given grid point.

$$Wt = \begin{cases} (1+R/D)^{-2} & \text{for } R \leq C \\ 0 & \text{for } R > C \end{cases} \qquad (2)$$

R is distance from the datum to the grid point in degrees and D is a measure of the width of the weighting function. C is the "cut off" distance. Fig. 4 also shows the cloud field contains less small-scale structure than the ship observations. The gridding scheme should affect the resulting cloud motion field little since, as shown in Fig. 4, the weighting function is somewhat narrower than the spatial correlations.

The above result suggests that if the scatterometer had a moderate skill for determining the correct wind direction, one could use the scatterometer's skill with an iterative process to determine wind direction. For example, if 1° binning in the scatterometer data is used
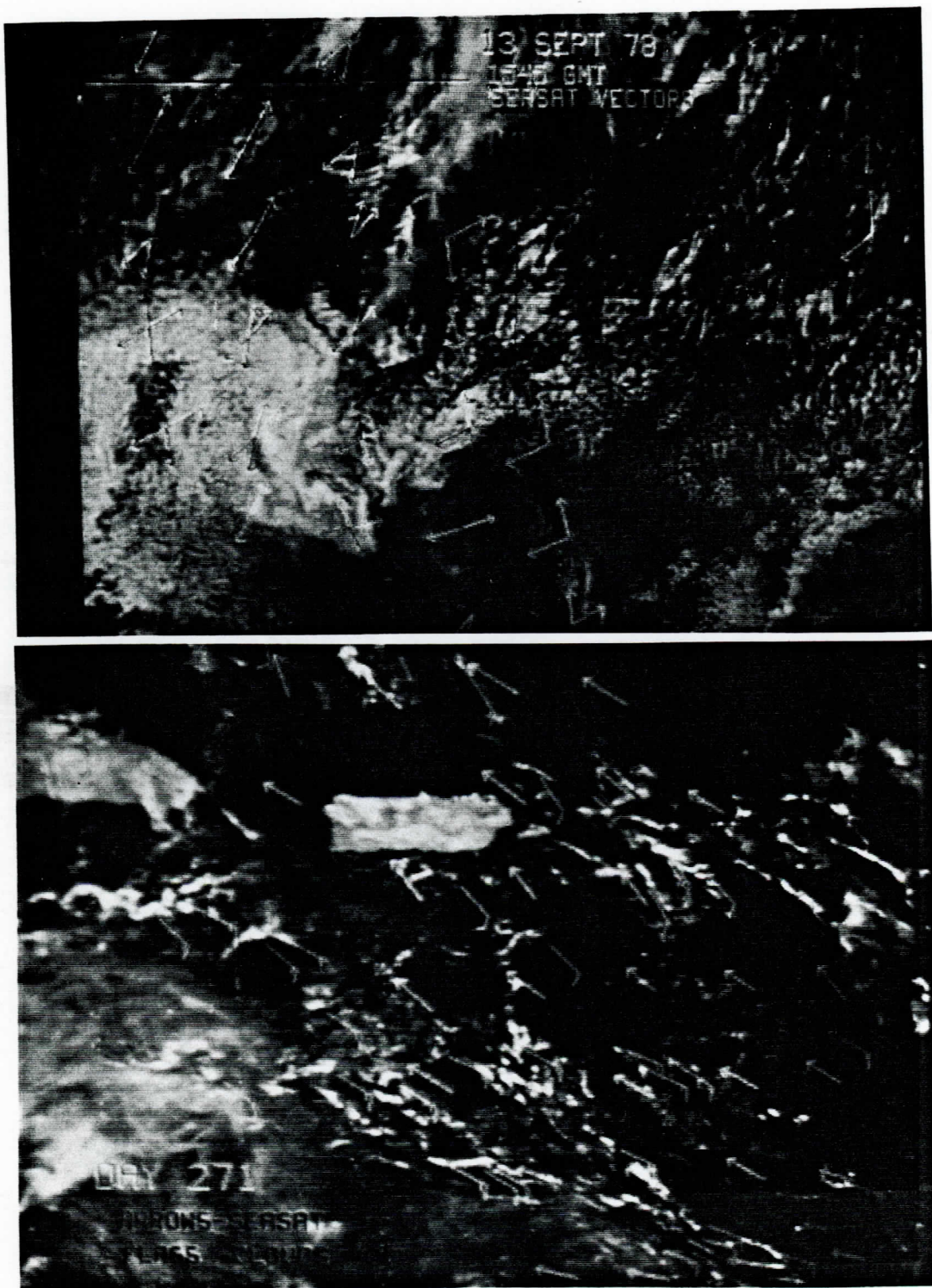
14

Fig. 3.   Alias removal. The top panel shows a typical example of
ambiguous vectors; most are fourfold, a few twofold. On the original
photograph, the solutions of different rank are in different colors
which do not reproduce equally well in black and white.   The lower
panel (from a different day) shows how cloud motions (meteorological
wind flags) have been used to select those vectors having the same
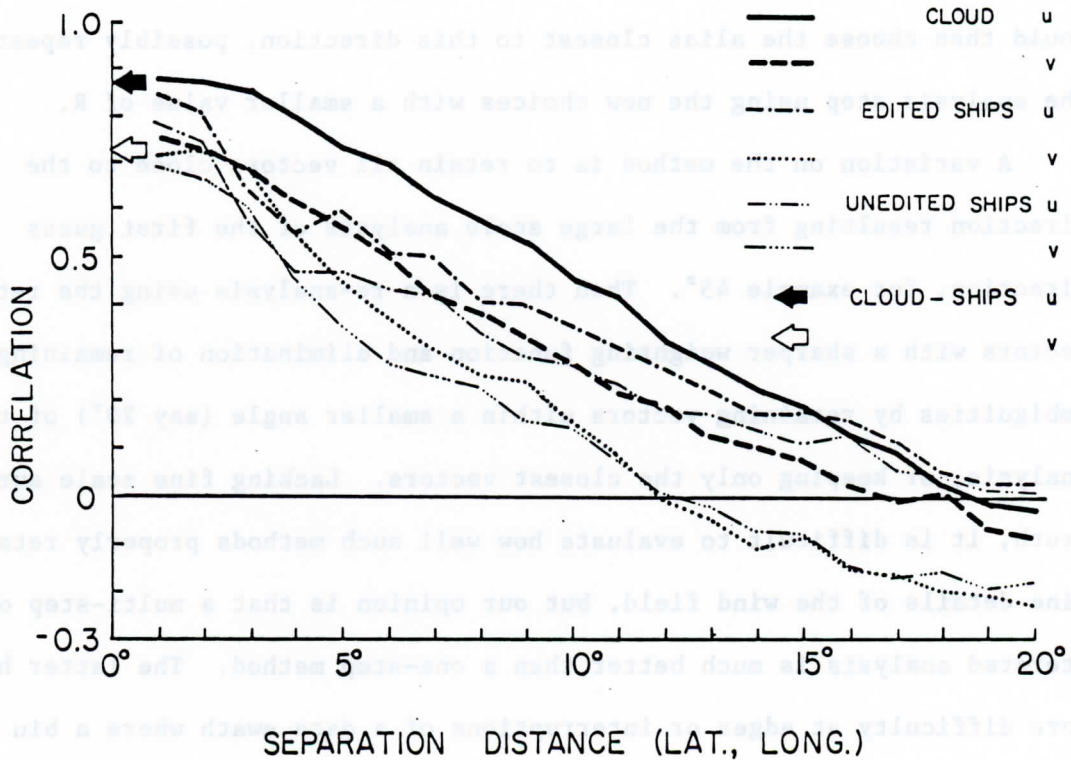general directions.

Fig. 4.   Correlation between pairs of observations as a function of spatial separation.

and if these were re-gridded using (2) with R about 4°, each resulting grid point is influenced by about 36 bins, but strongly influenced by about 16 of them.

If the scatterometer had slight skill, the vector mean of the first choice aliases would be close to the <u>direction</u> of the correct alias. One would then choose the alias closest to this direction, possibly repeating the analysis step using the new choices with a smaller value of R.

A variation on the method is to retain all vectors close to the direction resulting from the large scale analysis of the first guess direction, for example 45°. Then there is a re-analysis using the retained vectors with a sharper weighting function and elimination of remaining ambiguities by retaining vectors within a smaller angle (say 20°) of the analysis, or keeping only the closest vectors. Lacking fine scale surface truth, it is difficult to evaluate how well such methods properly retain fine details of the wind field, but our opinion is that a multi-step or iterated analysis is much better than a one-step method. The latter has more difficulty at edges or interruptions of a data swath where a bin may not be surrounded by other bins, so that not as much information is available to influence selection of its direction. After two steps, information has propagated outward to fix these directions, and subsequent steps usually produce no further changes.

After a single step, in addition to the edge problem, the analysis may be "kinky" in a few small regions where there were small clusters of first choice vectors which were incorrect choices. After two steps, these are almost always replaced with the same vectors that an analyst would choose subjectively. Such schemes would work in areas where the wind is uniform or changes direction smoothly. Reliance on cloud motions would then be

17

relegated to areas of sharp change, such as fronts, confluences, small vortices, and the like.

Unfortunately, as shown in Fig. 5, the data in the Interim Geophysical Data Record had insufficient skill to use a self starting method as outlined above. However, this scheme has been successfully tested for model simulated scatterometer data for incorporating an improved antenna system (Schroeder et al. 1983)

As long as a large scale reliable first guess of the direction is available, it can be gridded and used in the manner just discussed. Our research showed that an analysis of cloud motions would work. We conjecture that at polar and midlatitudes, where the geostrophic relation can be trusted, geostrophic directions from a pressure analysis (after an adjustment for cross isobar flow) as well as ship wind directions could be used. However, since the intended purpose of remotely sensed winds is to obtain data in regions poor in surface data, these are not of practical help. The obvious remaining choice would be geostrophic winds (with an adjustment for cross-isobar flow) from an analysis of satellite sounding data. Twomey (Hayden et al., 1979) gives a technique for determining the vertical resolution for any temperature retrieval algorithm and set of measurements. Figure 6 is an example of a Twomey analysis on a set of instruments resembling those on U.S. polar orbiting satellites (Hayden et al., 1979). A number of curves are shown corresponding to temperature delta functions applied at the levels indicated beside the curves. The shape of each curve represents the vertical resolution relative to temperature at the indicated level.

Figure 6 suggests the lowest level on these soundings is somewhat too high and too deep, so they should be reserved for areas where no low level clouds can be seen.
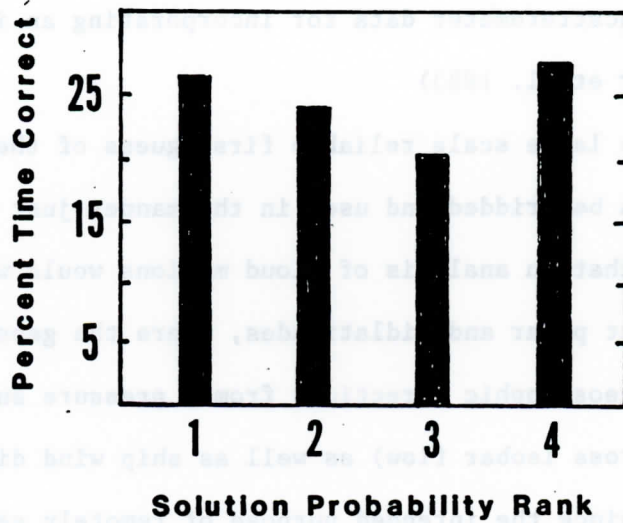
Fig. 5.   Scatterometer directional skill. This figure shows the relative
           frequency with which the alias selected with the help of cloud
           motions corresponded to the probability rank òf the alias in the
           interim geophysical data record for a 7-degree of arc long
           segment of pars 1339. Some segments show higher skill -- usually
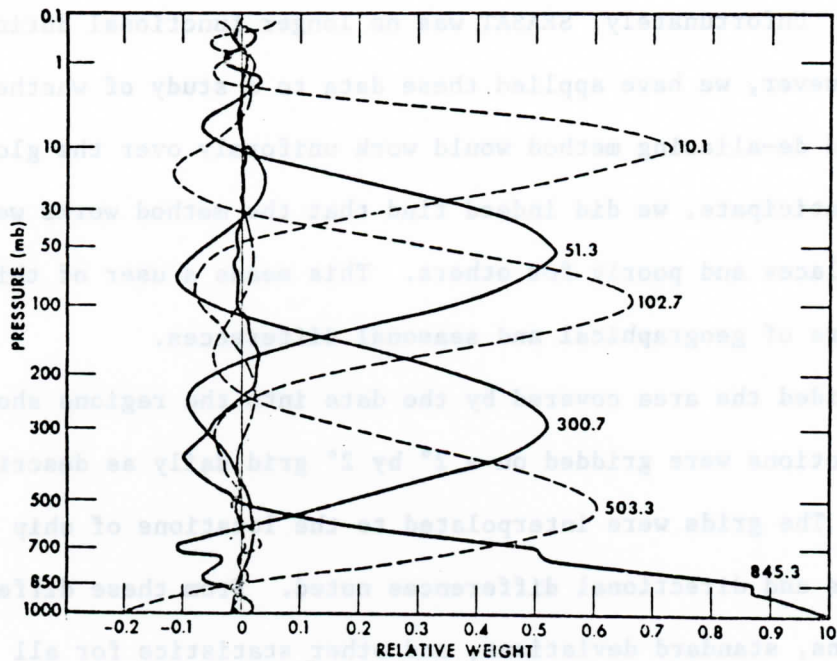   when only two aliases are presented.

19

Fig. 6. Estimates of the vertical resolution of satellite-derived
temperature profiles by the Twomey method. Curves indicate
vertical averaging for estimating temperatures at discrete
pressure levels as noted by numbers at each peak.

3.4 Applicability of the Method to Various Regions

For another research program we obtained a large volume of cloud
motion and surface ship observations during the 1979 Global Weather
experiment. Unfortunately, SEASAT was no longer functional during this
period. However, we have applied these data to a study of whether a cloud
motion-based de-aliasing method would work uniformly over the globe. As
one might anticipate, we did indeed find that the method works well some
times and places and poorly for others. This means a user of this method
must be aware of geographical and seasonal differences.

We divided the area covered by the data into the regions shown in Fig.
7. Cloud motions were gridded on a 2° by 2° grid daily as described above
using (2). The grids were interpolated to the locations of ship
observations and directional differences noted. From these differences we
derived means, standard deviations, and other statistics for all
comparisons within each of the numbered geographical boxes. The results
are summarized in Table 5 which shows the root mean square deviation of the
veering angle from the mean, for each box, by season and cloud motion
direction.

Using 45° rms veering as a usability criterion, we see that the
poorest area is box 3 for all seasons. About 92% of the vectors are in
categories showing large dispersion. Possibly summer winds from the
northern quadrant have usable skill; otherwise, only easterly winds with
speeds over 10 ms^{-1} should be trusted. In box 6, low speed easterlies in
summer and winter were marginally poor. We were somewhat surprised that
summertime low speed winds in box 12 showed dispersions above 52°.
Similarly, southerly fall winds deviated about 59°. Box 15 was well
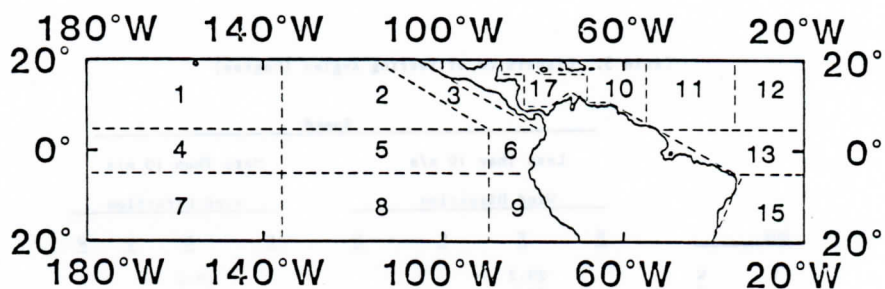behaved except for the 11% of winter winds out of the north quadrant. In

21

Fig. 7. Key to the boxes listed in Table 5.

Table 5. Dispersion of Veering Angles (Degree)

BOX		Speed							
		Less Than 10 m/s				More Than 10 m/s			
		Wind Direction				Wind Direction			
		N	E	S	W	N	E	S	W
1	W		29.2				19.2		
	S		27.5				16.6		
	F		30.6				11.7		
2	W		38.5				18.3		
	S		34.1				27.0		
	F		37.1				17.7		
3	W	47.5	55.6	116.8			30.7		
	S	44.1	85.5	65.8	64.3		45.3		
	F	51.8	62.2	74.4	51.5				
4	W		30.1				16.7		
	S		26.6						
	F		18.8						
5	W		22.6				22.2		
	S		19.1				11.7		
	F		36.1						
6	W		51.9	20.3					
	S		34.0	27.9			16.3		
	F		45.5	22.8	26.1				
7	W		25.6						
	S		32.7						
	F		30.0						
8	W		19.7				22.7		
	S		40.0						
	F		17.9						
9	W		23.6	23.3			20.8		
	S		25.6	15.7			14.5		
	F		21.9				17.3		
10	W	19.1	27.5				21.6		
	S		33.5				17.1		
	F		27.2				18.2		
11	W	17.6	28.5				24.0		
	S		37.0				21.4		
	F		36.5				16.4		
12	W	32.5	27.8						
	S		52.0	62.2	67.5		17.8		
	F		43.9	59.1					
13	W	42.0	31.3	35.4		33.0	26.7		
	S		27.6	27.2			17.3		
	F		21.8				14.1		
15*	W	65.9	29.7						
	S		25.4	25.8			18.0		
	F		21.7				16.3		
17	W	48.6	27.8			25.8	18.8		
	S		29.8				22.0		
	F	84.4	40.3	49.7	61.3		19.4		

* Boxes 14 and 16 were not used in this study

23

box 17, 92% of winter winds, 100% of summer winds, and 74% of fall winds were in usable classifications.

From Figs. 8a and 8b, we can see that there are relationships between rms deviation of the veering angle and steadiness and speed -- both obtained from the surface observations. In this context, steadiness is the magnitude of the average wind vector divided by the average speed. However, these two relations (Figs. 8a,b) are not entirely independent since, as shown in Fig. 9, speed and steadiness are related.

It should be borne in mind that the deviations cited above necessarily incorporate the observational errors in the ship winds. The plots in Fig. 10 suggest the rms error of the directional measurement of a single ship is about $40°/2^{\frac{1}{2}}$ or $28°$. Hence, the results in Table 5 necessarily lie on the pessimistic side of the truth.

After the problems with the quality of ship observations are addressed, one would account for regional-seasonal differences of Table 5 on the basis of boundary layer differences. This is beyond the scope of this report except for a few remarks. Based on a still incomplete study aimed at producing a statistical boundary layer, the factor of overriding significance is air sea temperature differences. In mid-ocean regions, air temperature reflects the pattern of ocean temperatures. Thus, through advective processes, the ocean temperature field couples with wind speed and direction to modulate the air-water temperature difference. In some regions, there are strong constraints due to orography and land sea temperature differences. Box 3 is an example. There are also regions where the comparisons are affected by the tendency of vessels to remain just outside territorial limits which accentuates the thermal or sheltering effect of the land.
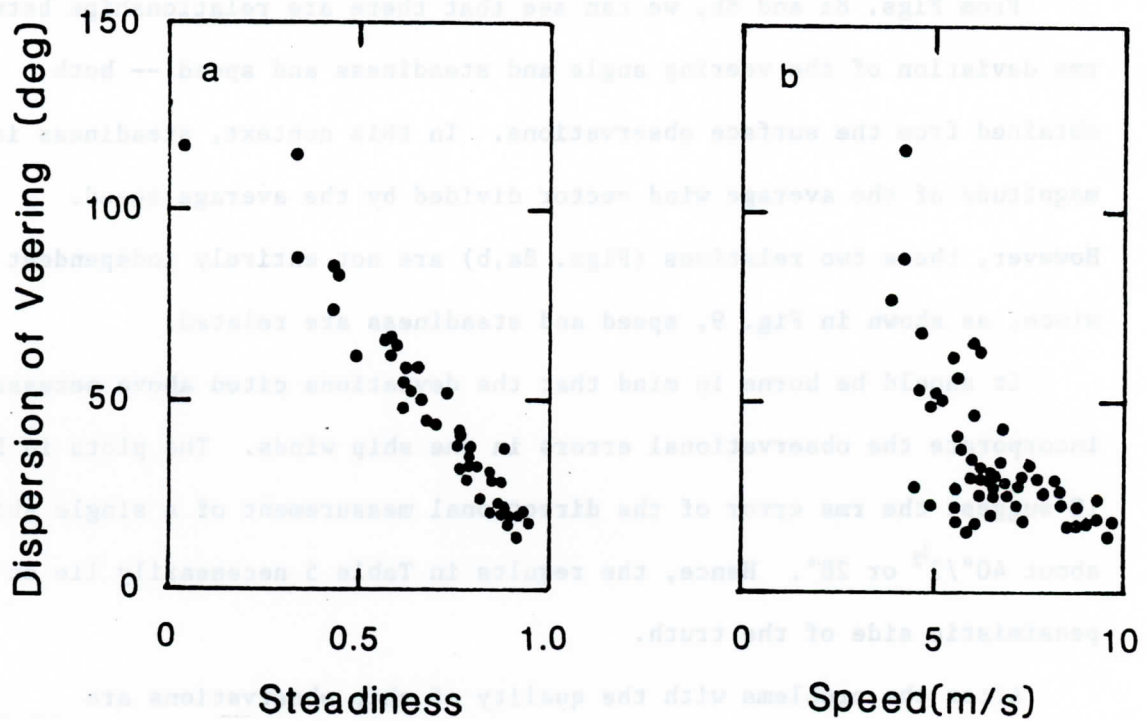
24

Fig. 8. Relations between speed and dispersion of the veering angle, and between steadiness and dispersion of the veering angle for the area shown in Fig. 7 during January, February, June, July, and August 1979.
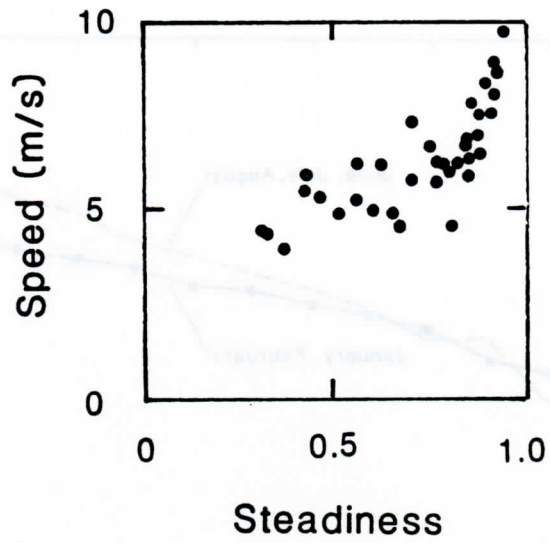
Fig. 9.   Relation between speed and steadiness. The data
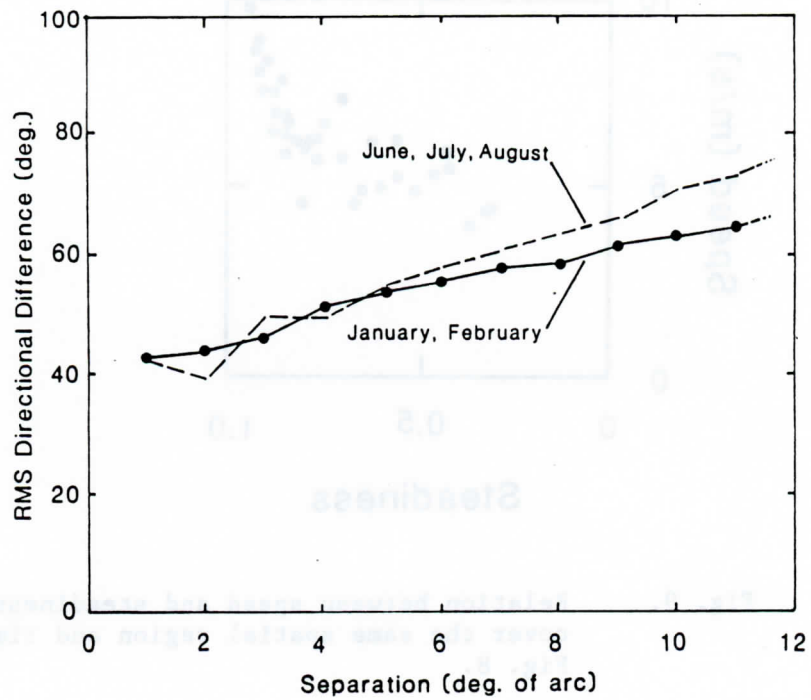cover the same spatial region and time period as
Fig. 8.

Fig. 10. Growth of directional differences between pairs ship wind observations with increasing separation between the ships. One degree of arc is about 110 km. The data come from the region shown in Fig. 7.

4. A Case Study Using Scatterometer Data

4.1 Storm Hope

As a demonstration of the potential for monitoring storms over oceans using satellites, we studied one storm in the North Atlantic for a period of four days. Tropical storm Hope was chosen for our pilot study because it traversed an area rich in ship data, and SEASAT was taking data over the Atlantic as part of its demonstration tests. At the same time, the eastern GOES-E was providing cloud imagery of the same area for routine weather observations.

Storm Hope originated on about the 12th of September 1978 off the coast of South Carolina at 32°N and 77°W. The storm moved to the east and reached tropical storm status on 17 September. Hope generally followed a boundary between the tropical air and ocean to the south and the colder sub-polar conditions to the north (Figs. 11, 12, and 13). This was evident from the temperature analyses made of the area for a four-day period during the growth of Hope. To the south of Hope, ocean surface and air temperatures from 26°C to 28°C were found with very small gradients over the area south of 30°N. To the north of Hope's track, the temperatures of both the ocean and the atmosphere decreased sharply with latitude. The northern boundary of the Gulf Stream from the NOAA/NESS satellite analysis also is indicated. These patterns depict a "polar front", so to speak, in both the ocean and the atmosphere at the latitude of storm Hope.

4.2 Data and Analysis

To analyze the air and water temperatures at the ocean surface around storm Hope, we used observations of the merchant ships. Because there was a lot of noise in these data and their coverage was thin in some areas, a compositing technique had to be used. All the ship reports for a four-day
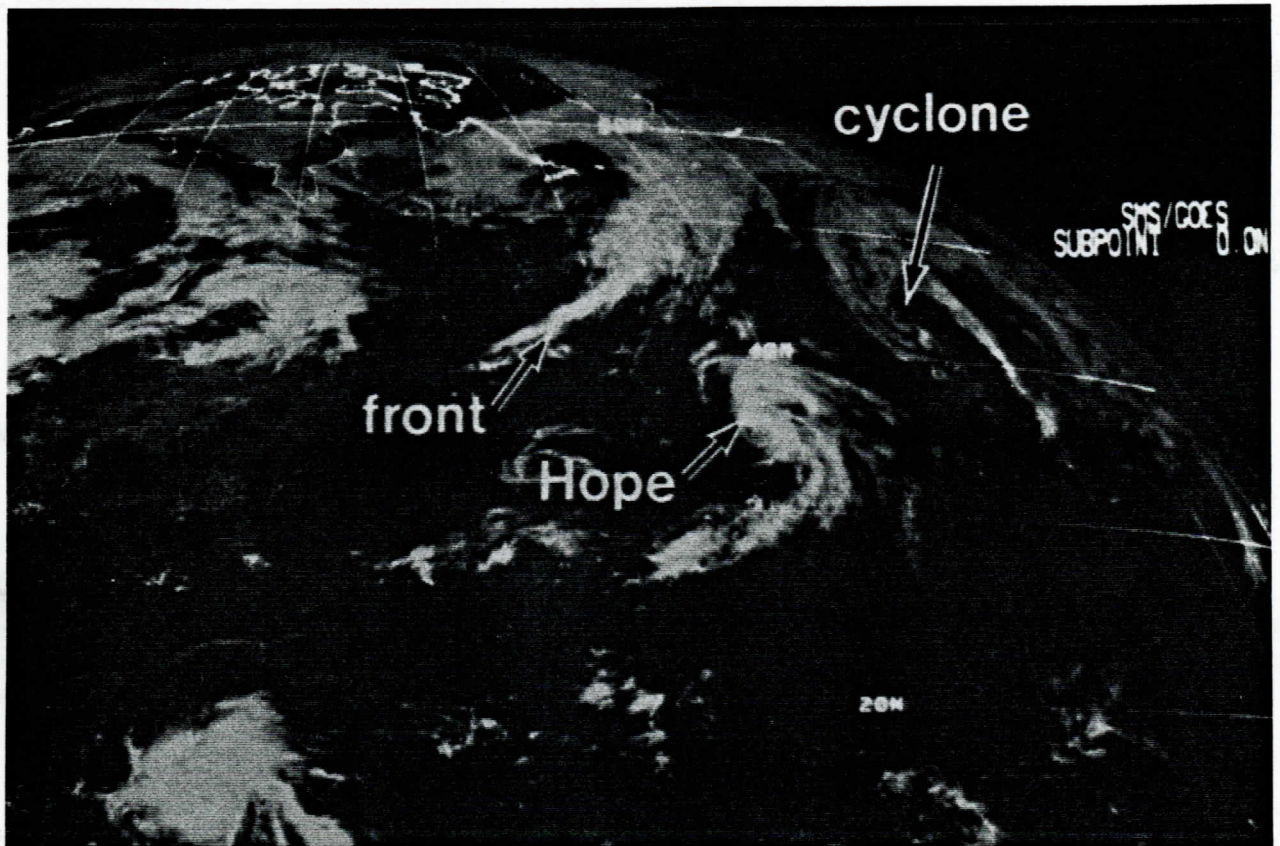
28

Fig. 11.   A GOES-East image of the North Atlantic on
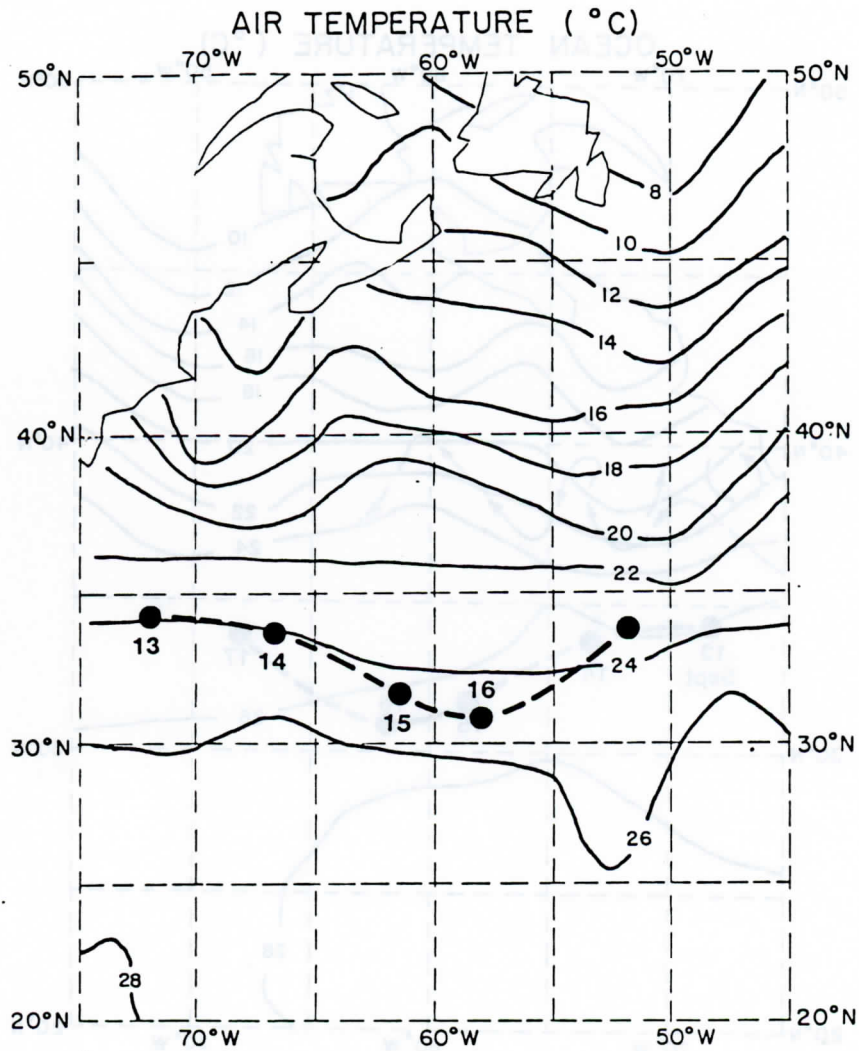1700 GMT 17 September 1978.

Fig. 12. A composite surface air temperature analysis for the
North Atlantic made from all ship reports from 00 GMT
14 September to 1200 GMT 17 September 1978. The track
of tropical storm Hope from 13 September to 17 September
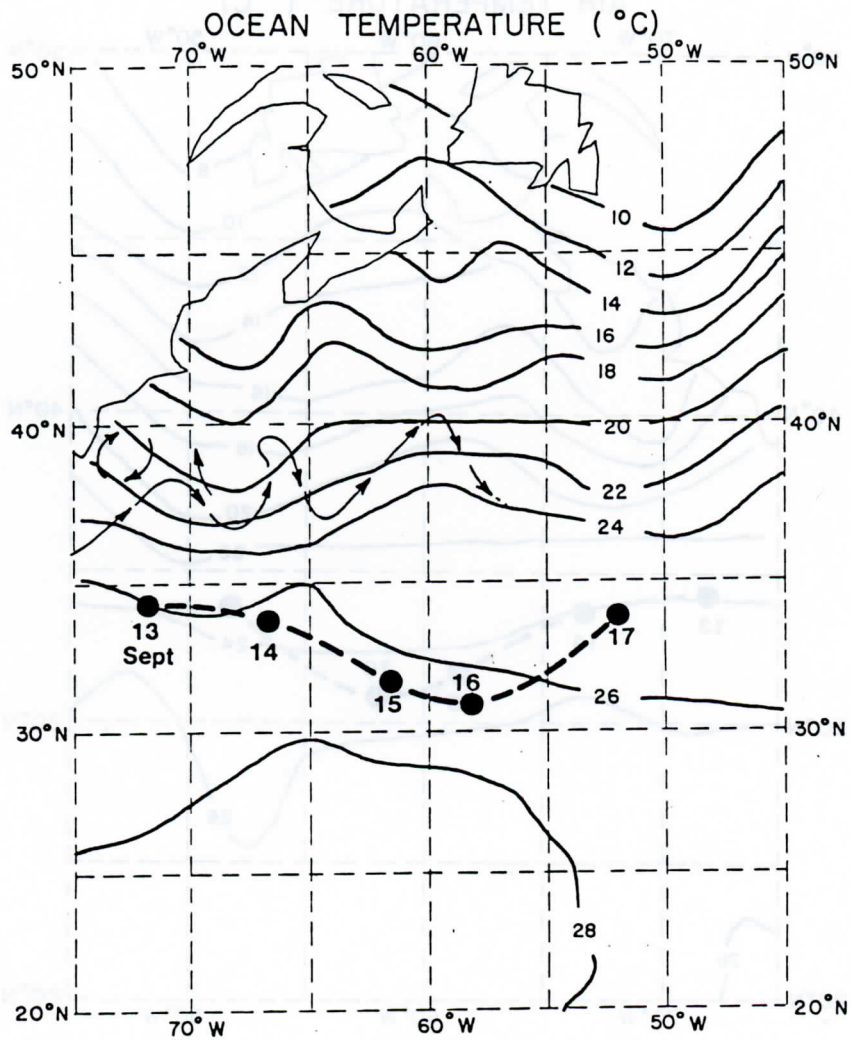is indicated by the bold line.

30

Fig. 13. A composite surface ocean temperature analysis for
the North Atlantic made from all ship reports from
00 GMT 14 September to 1200 GMT 17 September 1978.
The arrows depict the northern boundary of the Gulf
Stream from the NOAA/NESS Gulf Stream analysis
17-20 September 1978.

31

period, both 00Z and 12Z, were interpolated to a 1° latitude and longitude grid for the area shown in Figs. 12 and 13. The observations were averaged together for all four days. Their areal distribution is shown in Figure 14.

Weights were used to accentuate the observations closest to each grid point. The weights were defined as in (2) with D = L, and C = 4. for the four days, a total of 430 observations were obtained in the area.

To estimate the stability of the atmospheric boundary layer, the ocean temperature grid was subtracted from the air temperature grid (Fig. 15). This analysis indicated that the conditions around Hope ranged from neutral to slightly unstable south of the storm and to very unstable north of the storm. No stable conditions were found near the storm. The tropical area south of the storm had an air-water temperature difference of −1° over most of the area which is typical of tropical areas. North of the storm, however, the air-water temperature differences were much larger with the most unstable area being located around 38°N and 54°W.

The wind field around the storm was analyzed from the combined observations from three sources: ship reports, the SEASAT active microwave scatterometer, and cloud motions. The SEASAT SASS directional ambiguities were removed using cloud motions.

On 15 September, a SEASAT orbit crossed directly over the storm (Fig. 16), providing observations both in the tropical air south of the storm and in the unstable air north of the storm. A second orbit also was examined on 16 September. This orbit, unfortunately, missed the storm center and only made observations northeast of Hope (Fig. 17). However, it provided extensive observations in the cold surge that followed the cyclone to the east of Hope.
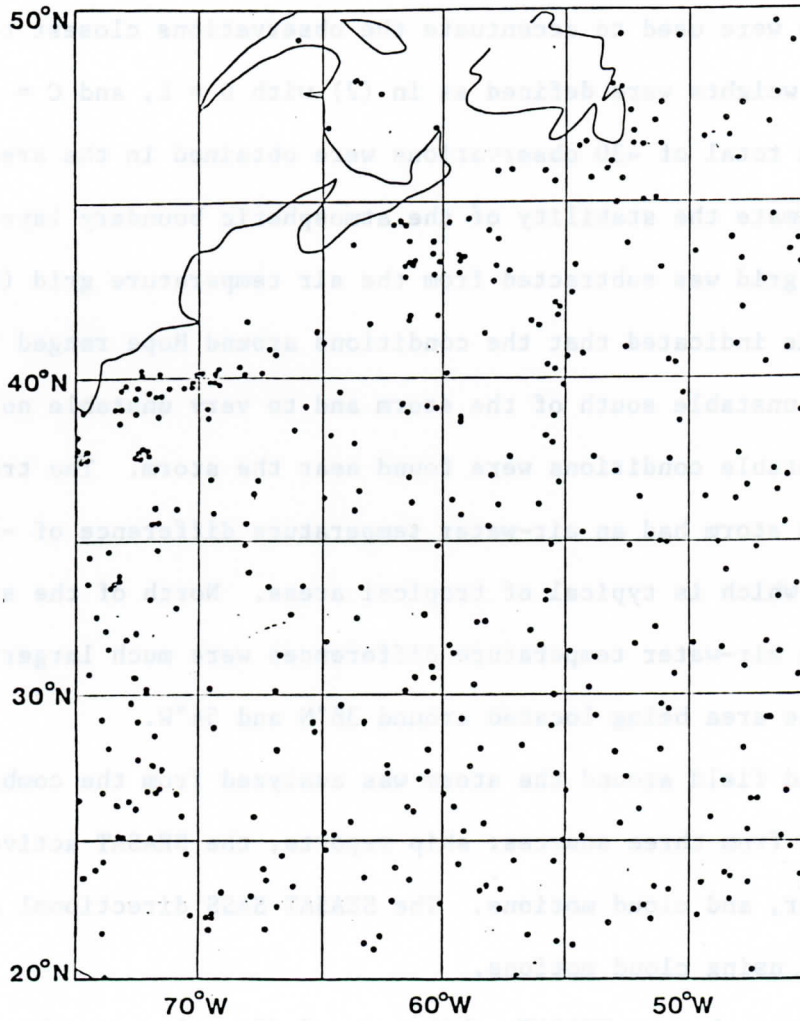
32

Fig. 14.   The locations of the ship reports used for the
temperature analyses from 14 to 17 September 1978,
for both the 00 and 1200 GMT observation times
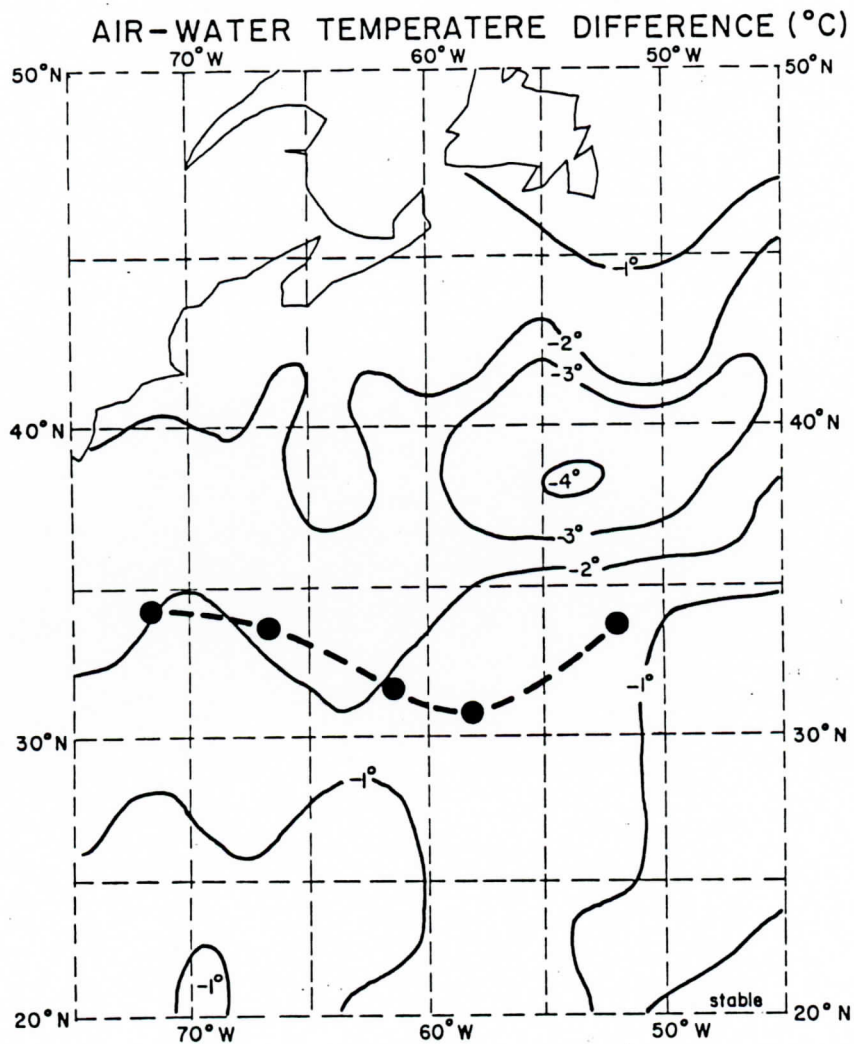combined.

Fig. 15. The difference between the air and water temperatures
using the analyses shown in Figs. 12 and 13.
Negative values indicate the air temperature was
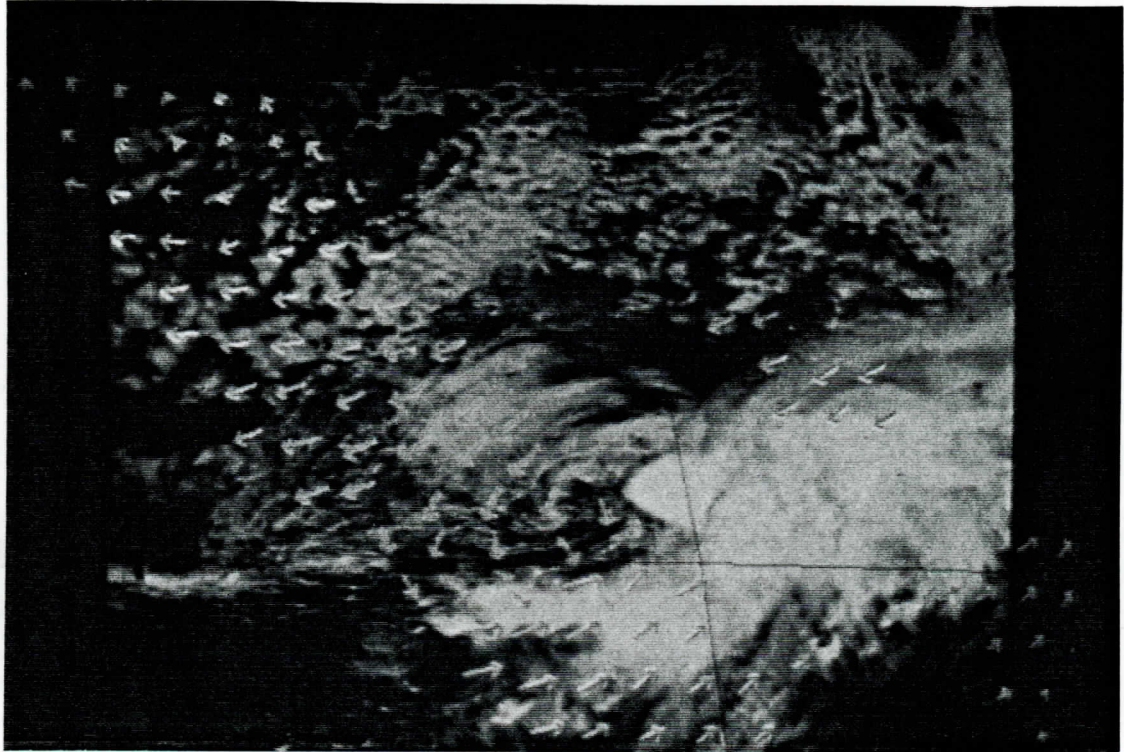< the water temperature.

34

Fig. 16.   SEASAT SASS wind estimates of the North Atlantic over storm Hope.
The SEASAT satellite crossed the equator at 1310 GMT,
15 September 1978 heading north.   The background image is
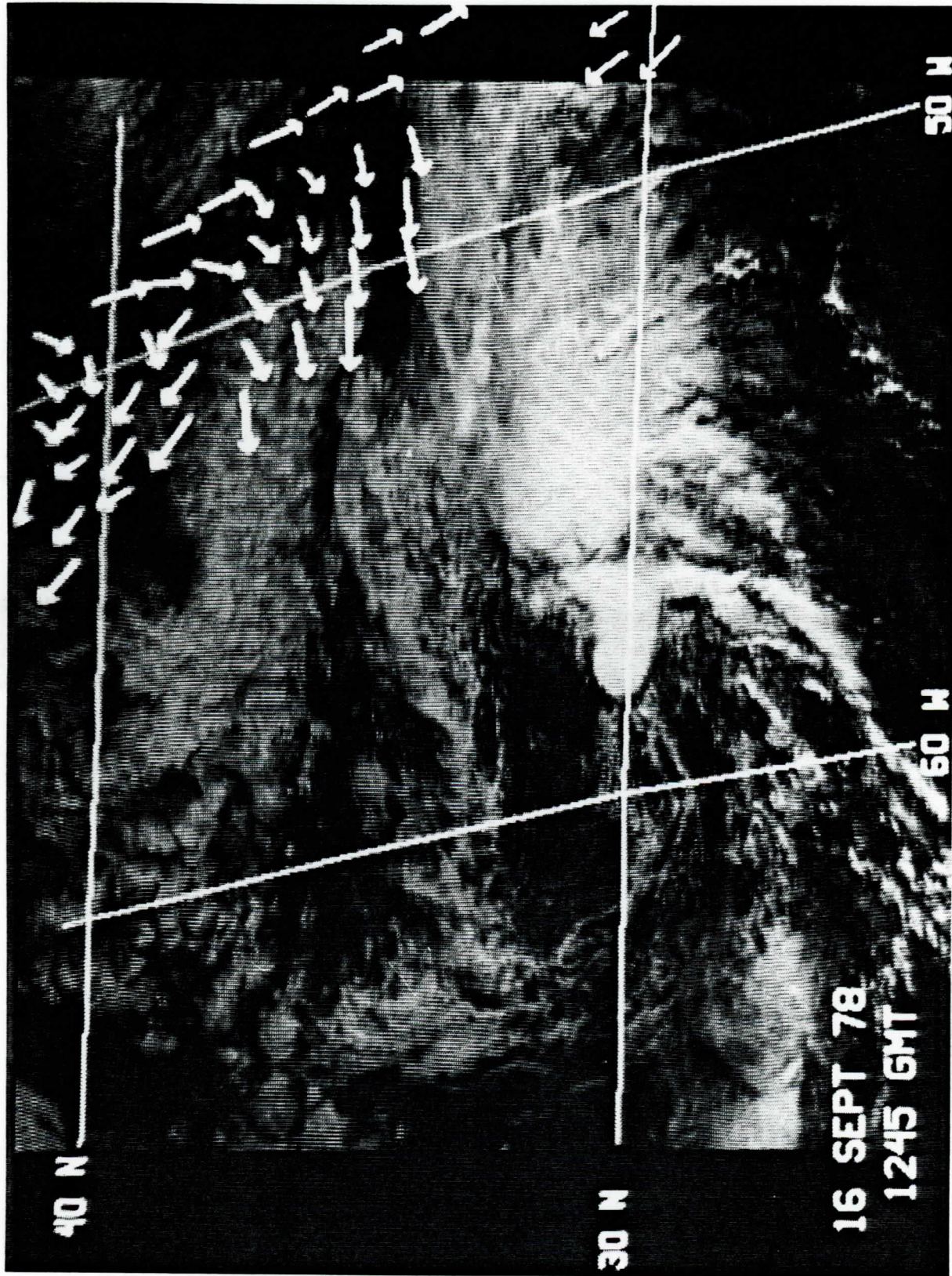the GOES-East visible channel image of the area made at 1300
GMT.

Fig. 17. SEASAT SASS wind estimates plotted on the GOES-E visible image for 16 September 1978. The SEASAT crossed the area at 1245 GMT while the GOES image was taken at 1200 GMT.

During this period the SEASAT SASS often sampled on only one side of the satellite's orbital track. This nonsymmetrical sampling pattern was used to experiment with higher resolution coverage in a smaller area (half degree binning). The consequences of this mode were large gaps between orbital tracks, which made coverage more difficult. During the period of 15 to 17 September, only one SEASAT orbit provided direct coverage over the storm's center during the daytime.

The cloud motion coverage was extensive, both north and south of the storm (Figs. 18 and 19). The only area poorly covered by cloud motions was east of the storm where the low level clouds could not be tracked under cirrus.

Cloud patterns seen on the GOES images indicated the different atmospheric boundary layer conditions north and south of the storm (Figs. 18 and 19). South of the storm, the low clouds were found in small groups. (Individual cumuli cannot be resolved with these images.) North of the storm, cellular patterns were evident resembling those commonly observed where unstable boundary layers exist (Agee 1973). The cloud motion observations indicate that the cold flow northeast of Hope turned from northwesterly winds to easterly winds. Thus, cold air continued to cross warmer waters as the air circulated around the storm.

To the south of Hope, a strong southwesterly flow was evident. The cloud patterns in this area were typical of the patterns commonly observed in tropical areas -- small cloud groups at non-uniform spacings. West of the storm, a line of clouds can be seen where the northeasterly cloud motions turned to southwesterly motions. A strong wind directional shift was apparent along this line. (See Figures 15 through 19.)
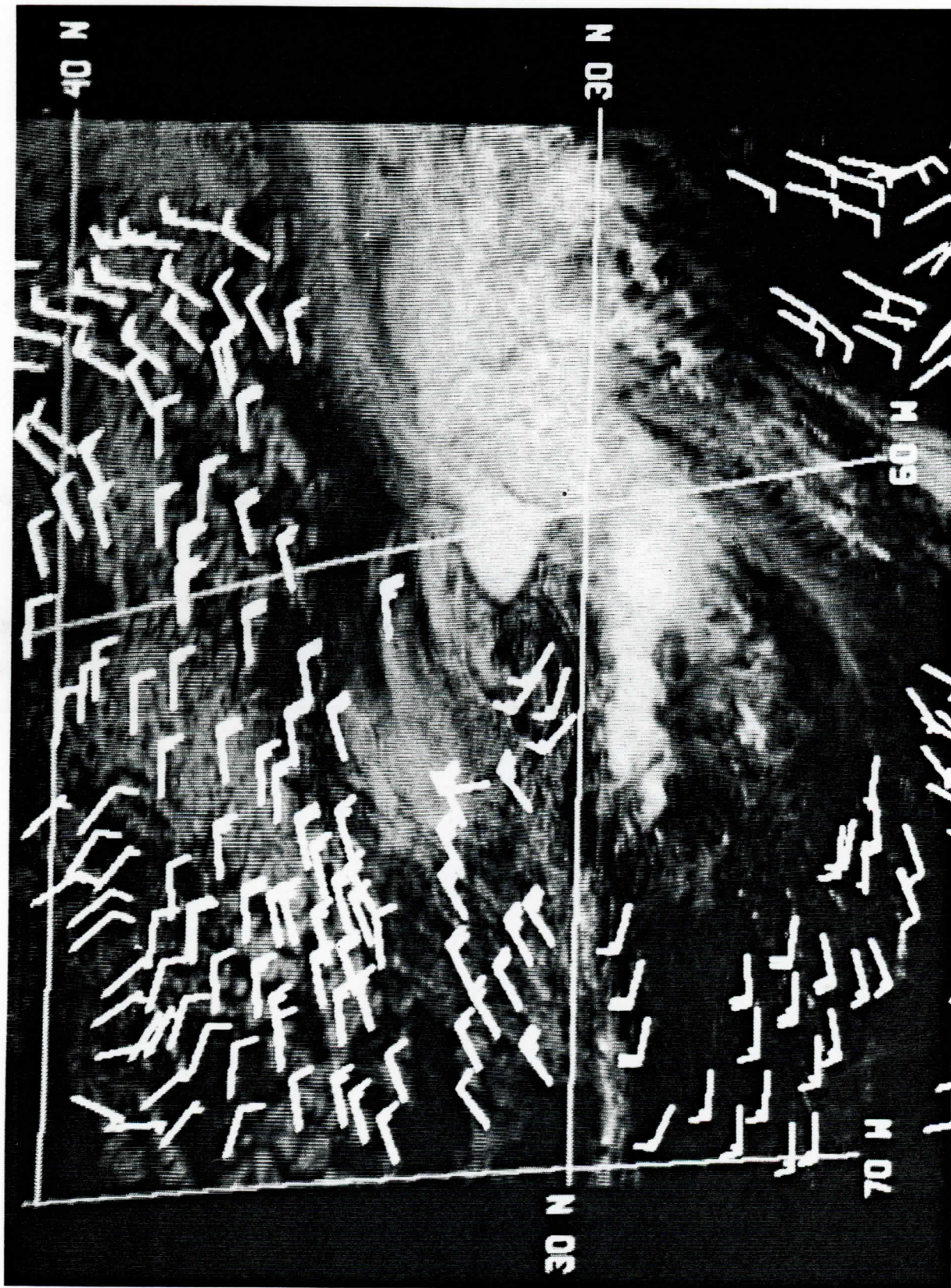
Fig. 18. A GOES-E image of storm Hope 1300 GMT, 15 September 1978 with the cloud motion vectors imposed. The cloud motions were tracked on three GOES images from 1300 to 1400 GMT.
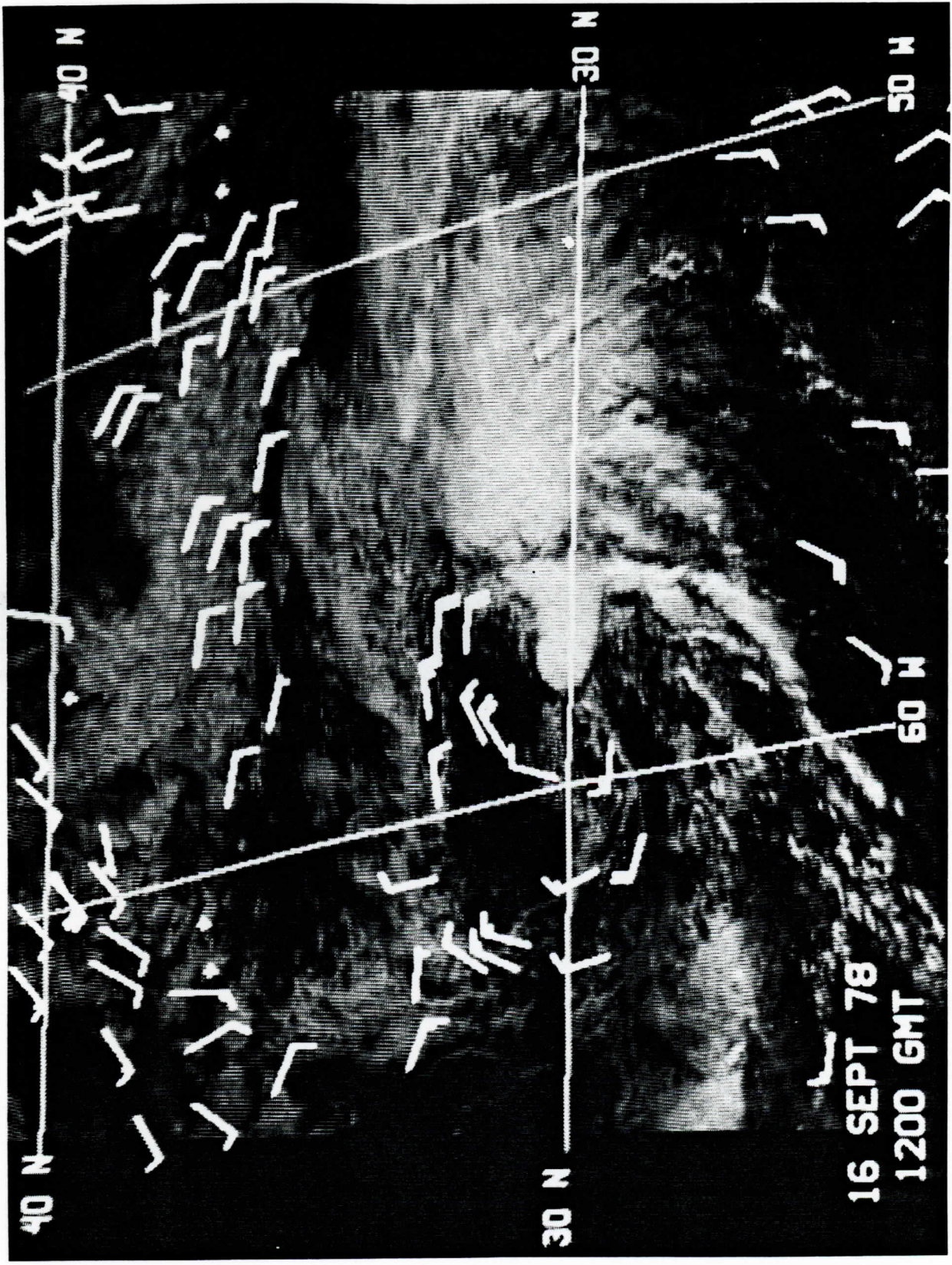
Fig. 19. A GOES-E image of storm Hope with the cloud motions imposed for 16 September 1978. The cloud motions were measured from 1200 to 1300 GMT.

4.3 Boundary Layer Effects

After ambiguity removal, the biases among the data sets had to be identified and removed. To quantify biases, SEASAT and cloud motions within 1° of latitude or longitude were compared. Results for the 15 and 16 September are shown in Table 6. Similar comparisons with ship observations were attempted, but too few co-located pairs were found. Ship reports often strongly disagreed with neighboring ships, as well as satellite observations casting doubt on many of the ship observations. We therefore have ignored the comparisons with the ship winds.

Atmospheric boundary layer wind shear can be different in different stability regimes. The cloud motion-SEASAT comparisons on 15 September were divided into two separate groups -- the very unstable area north of the storm and the tropical area south of the storm -- to isolate the different cloud motion-surface wind relationships.

North of Hope, we found very little shear between the cloud motion and SEASAT wind observations. Speed shears averaged less than 0.2 m s^{-1} while directional shears averaged between 1° and 9° of wind sheering (SEASAT dir. < cloud motion dir.). South of the storm, the speed and directional shears increased to 0.3 m s^{-1} and 11° veering on the average.

These comparisons are similar to the study of Wylie et al. (1981a), although the speed shears for tropical cloud patterns were slightly larger, ranging from 0.8 to 2.2 m s^{-1}. The lack of vertical shear where the cellular cloud patterns were found was also confirmed by the previous study.

The cloud motions north of the storm were not corrected for sub-cloud speed shear because of the results shown in Table 6 and the previous study. Wind directions, however, were given a slight correction of -3° north of the storm (based on Table 6) to better represent surface conditions.

40

Table 6. Mean differences between cloud motion and SEASAT wind observations. Differences are pairs within 1° latitude or longitude. The r.m.s. scatter is also shown.

Date and Location	Cloud Motion–SEASAT Winds	
	Speeds	Number of Vector Pairs
15 Sept north of storm	-0.1 ± 1.3 ms^{-1}	43
16 Sept north of storm	-0.0 ± 1.2 ms^{-1}	22
15 Sept south of storm	0.3 ± 1.8	12
	Directions	
15 Sept north of storm	$1° \pm 21°$	43
16 Sept north of storm	$9° \pm 57°$	22
15 Sept south of storm	$11° \pm 43°$	12

South of the storm, speeds were corrected by 0.7 m s^{-1} which is slightly larger than the results shown in Table 6. However, the Wylie et al. (1981a) study indicated stronger vertical shears under these conditions. The cloud motion directions were corrected by -16° based on the same studies.

4.4 Surface Wind and Transport Analyses

A combined wind analysis was made around Hope using all cloud motion, SEASAT, and ship data for 15 and 16 September. Only the 1200 GMT ship observations were used because these data had to be edited for spurious values using the cloud motion and SEASAT data. We limited our cloud motion analyses to the daytime visible images because smaller cloud groups could be tracked on these images than the infrared images.

All data were interpolated to a 1° latitude and longitude grid in the same manner as done with the temperature data. For the two days studied, 552 cloud motion vectors, 307 SEASAT vectors; and 148 ship reports were used. Four days had to be used for the temperature analyses because of the lack of satellite data. The wind analysis (Fig. 20) depicts the motions of the different air types around Hope more quantitatively than the individual SEASAT and cloud motion plots (Figs. 16-19).

The surface wind analysis (Fig. 20) was converted to a stress analysis using the bulk aerodynamic method

$$\tau = \rho_\alpha \, C_d U^2 \tag{3}$$

where the stress (τ) was calculated from the air density (ρ_α) and the wind speed (U) using a drag coeeficient (C_d). A drag coefficient that linearly increased with wind speed, $C_d = (0.8 + 0.065U)10^3$, was used as recommended by Wu (1980).
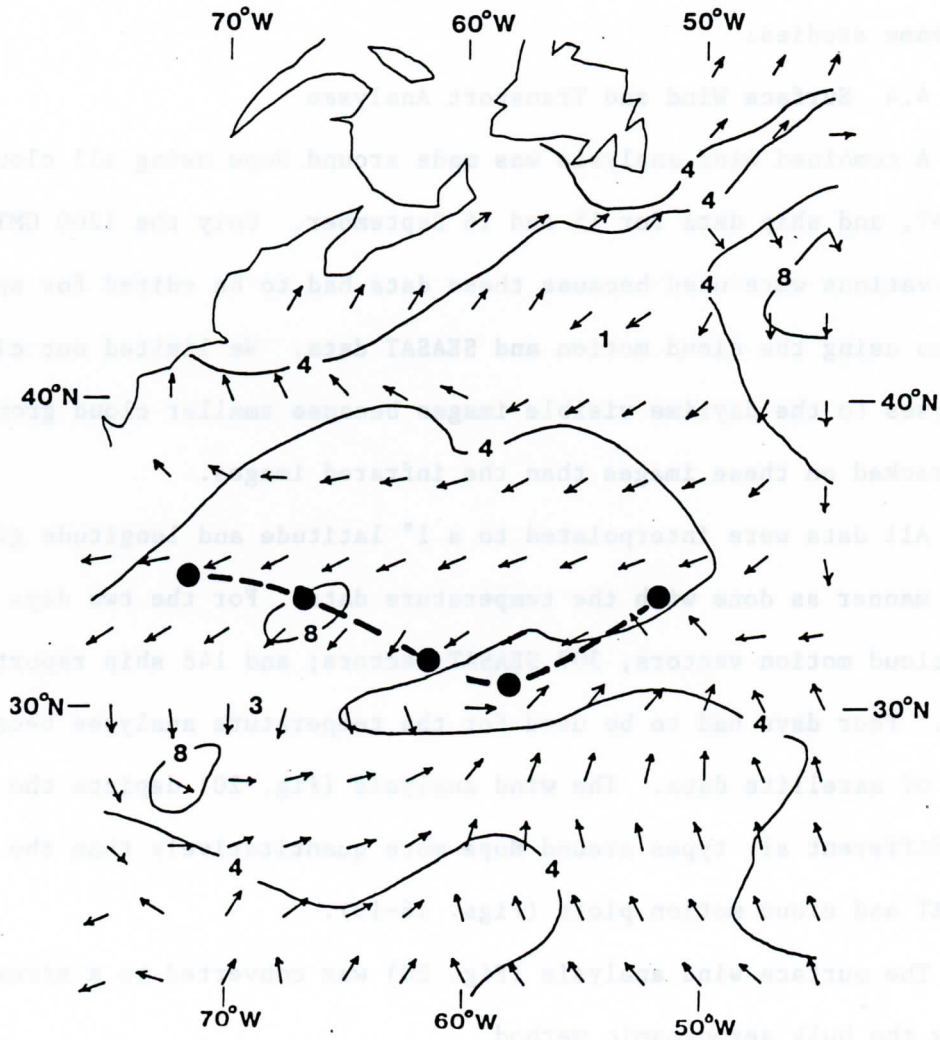
Wind Analysis

Fig. 20. Surface wind analysis for the North Atlantic made from the combination of cloud motion, SEASAT SASS and ship observations for 15 and 16 September 1978. The positions of storm Hope from 13 September to 17 September are indicated by the bold line.

The curl of the stress (Fig. 21) was strongly positive along the track of the storm as was evident in the wind plots (Figs. 16-19). The maximum value found was $56(10)^{-8}$ Nm^{-3} at 29°N and 72°W -- on the line where the easterlies curved to become westerlies in the wake of the storm. North of Hope, a moderately negative curl of $10(10)^{-8}$ Nm^{-3} was found while south of Hope, the curl was very small and only slightly negative.

Heat flux and evaporation around the storm were estimated using the ship and satellite data. The standard bulk aerodynamic formulae were employed.

$$HF = \rho C_\rho U(T_w - T_a) \tag{4}$$

$$Evap. = \rho L C_e U(Q_{ws} - Q_a) \tag{5}$$

Air and water temperatures (T_a and T_w) were taken from the ship analyses (Figs. 12 and 13) and combined with the wind speed (U) analysis previously shown (Fig. 20). The mixing ratio of the air (Q_a) was estimated as 80% of the saturated mixing ratio at the air temperature.

The transfer coefficients used ($C_h = 1.5(10)^{-3}$ and $C_e = 1.3(10)^{-3}$) were based on several previous measurements of these parameters reported in the literature. Studies in the tropics by Pond et al. (1974), Dunkel et al. (1974), and Hicks (1975) have found C_h to be approximately $1.5(10)^{-3}$. This value was confirmed by Francey and Garratt (1978) in the more unstable conditions found during AMTEX. In the North Atlantic, however, Smith (1980) found a lower value of C_h, $1.1(10)^{-3}$, using a large set of measurements. His study appears to be noticeably lower than the previous work. The same study of Smith (1980) found a drag coefficient (C_d) for stress that also was lower than most previous literature. We chose a value for (C_h) that had been repeatedly found by several studies.
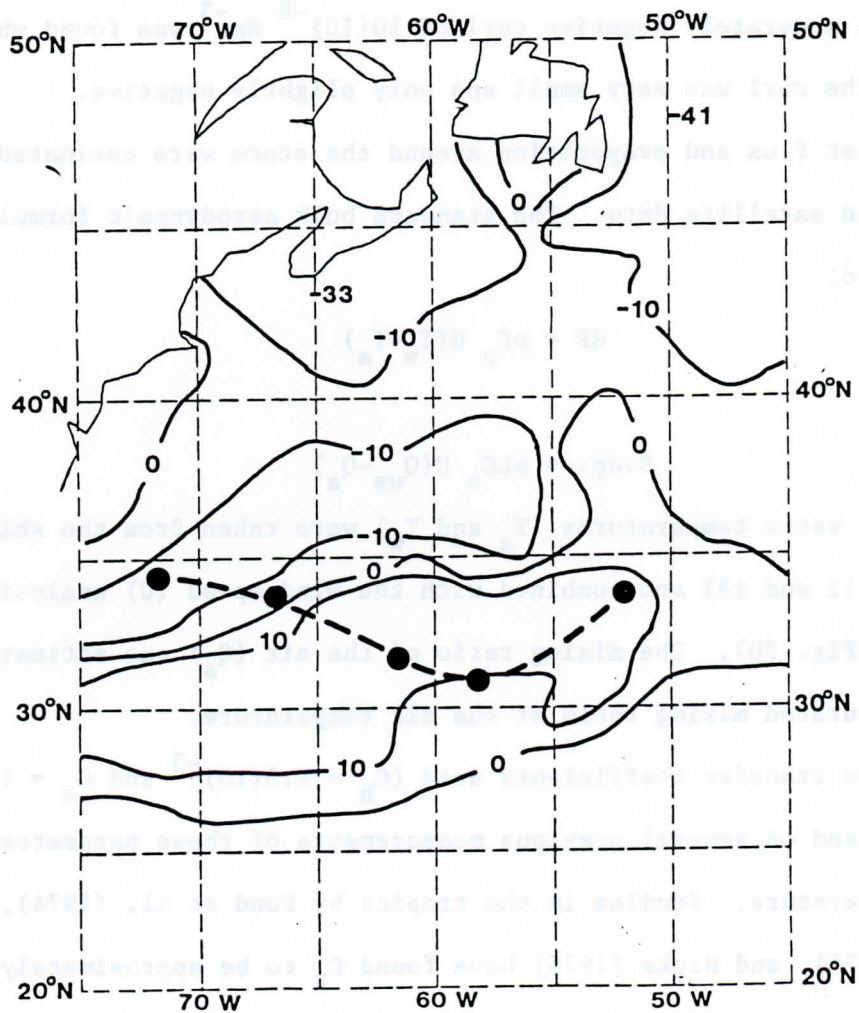
Fig. 21. The curl of the stress $\nabla \times \tau$ for the North Atlantic,
15 and 16 September 1978. Shading denotes areas where
a negative curl occurred.

According to Francey and Garratt (1978) and Dunkel et al. (1974), the evaporation coefficient (C_e) is less than the heat flux coefficient (C_h). The data base from which (C_e) has been calculated is smaller than (C_h) because of the difficulty in operating humidity sensors over the ocean. However, some studies such as Pond et al. (1974) and Hicks (1975) have found (C_e) to be nearly equal to (C_h). The exact magnitude of (C_e) is somewhat in doubt because of the variance between these studies and the small data bases used. The AMTEX data taken in unstable conditions (Francey and Garratt 1978) most resembled our study and thus we chose a value that roughly agreed with it.

The sum of the sensible and latent heat fluxes is shown in Fig. 22. The areas of strongest fluxes were also the areas where the highest wind speeds occurred -- the easterlies and the area where the easterlies curved to become westerlies. The cold surge ahead of the storm also is evident in the heat flux analysis around 42°N and 46°W.

Two separate sea surface temperature analyses were made, one for the period from 00 GMT on 14 September to 1200 GMT on 15 September (four observation times), and another from 00 GMT on 16 September to 1200 GMT on 17 September (also four observation times). The two analyses were then subtracted to show the change in the surface temperature pattern with time (see Fig. 23).

An east-west belt north of the storm's track cooled by 1° to 4°C in the interval between the two analyses, a two-day time span. This belt was approximately parallel to the storm's track. The southwestern end of the belt partially coincided with the area of maximum heat flux, around 36°N and 66°W. The largest ocean temperature change (-5°C) was found at 42°N and 52°W slighly north of where the largest air-water temperature

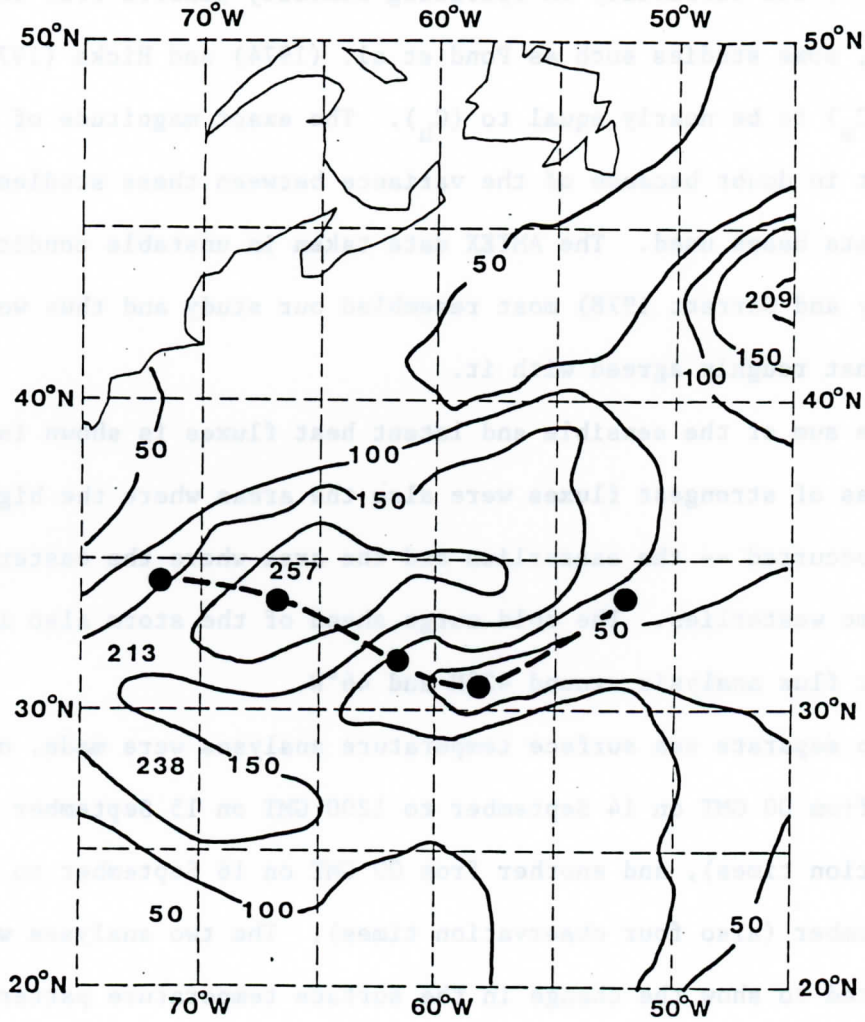Fig. 22. The combined sensible and latent heat fluxes from
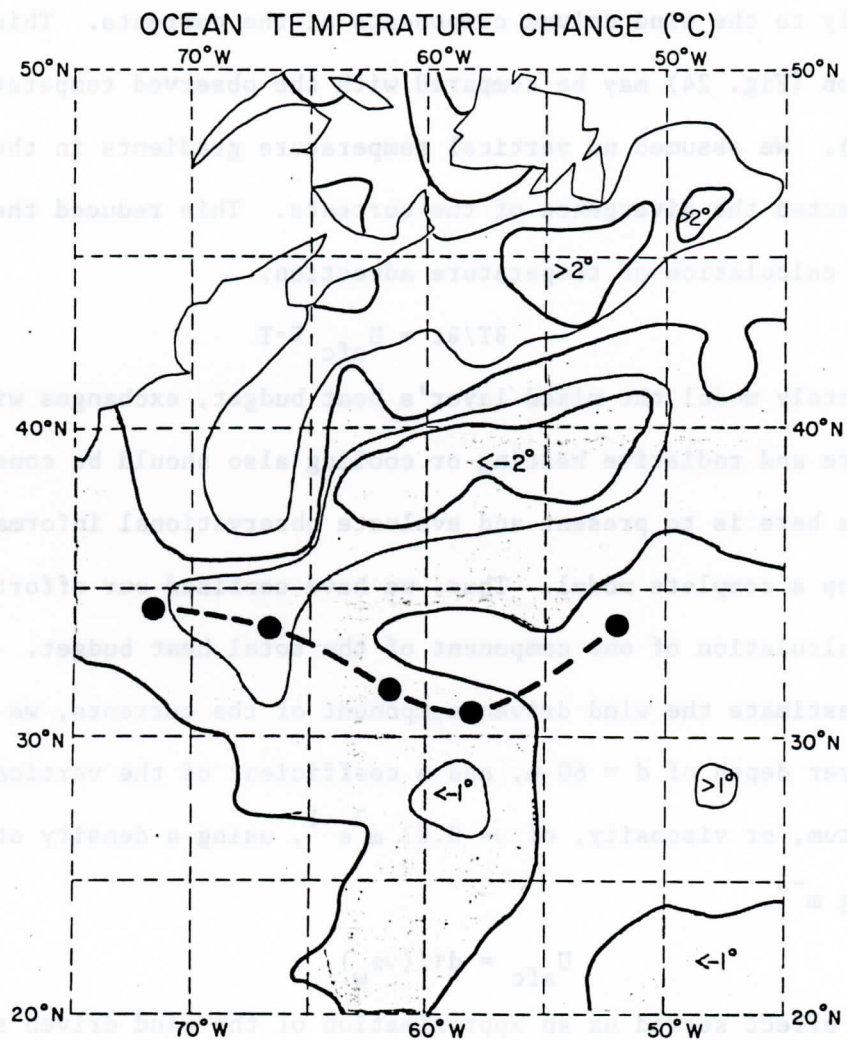the ocean to the air for 15 and 16 September 1978.

Fig. 23. The change in sea surface temperature between
two composite analyses made two days apart.
00 GMT 14 September to 1200 GMT
15 September 1978, and 00 GMT 16 September
to 1200 GMT 17 September 1978. Shading
denotes areas of temperature chages greater
than 2°C (warming or cooling).

differences occurred. However, this was upwind of where the maximum heat fluxes occurred.

We estimated what the changes in the surface temperature pattern were due solely to the wind driven components of the currents. This advective prediction (Fig. 24) may be compared with the observed temperature changes (Fig. 23). We assumed no vertical temperature gradients in the mixed layer and neglected the divergence of the currents. This reduced the problem to a simple calculation of temperature advection.

$$\partial T/\partial t = U_{sfc} \nabla \cdot T \tag{6}$$

To completely model the mixed layer's heat budget, exchanges with the atmosphere and radiative heating or cooling also should be considered. Our objective here is to present and evaluate observational information and not to develop a complete model. Thus, we have confined our efforts to a simple calculation of one component of the total heat budget.

To estimate the wind driven component of the currents, we assumed a mixed layer depth of $d = 60$ m, and a coefficient of the vertical exchange of momentum, or viscosity, of $\nu = 0.03$ $m^2 s^{-1}$, using a density of $\rho_\omega = 1000.0$ kg m^{-3}.

$$U_{sfc} = d\tau/(\nu\rho_\omega) \tag{7}$$

This, in effect served as an approximation of the wind driven surface currents using the wind analysis shown in Fig. 20 and the stress relationship (3). The current directions were assumed to be the same as the wind directions because of the short time scale involved (two days). Moreover, past observations have found only small veering angles between the surface winds and the surface currents (Kirwan, et al. 1979, and Pollard 1977).
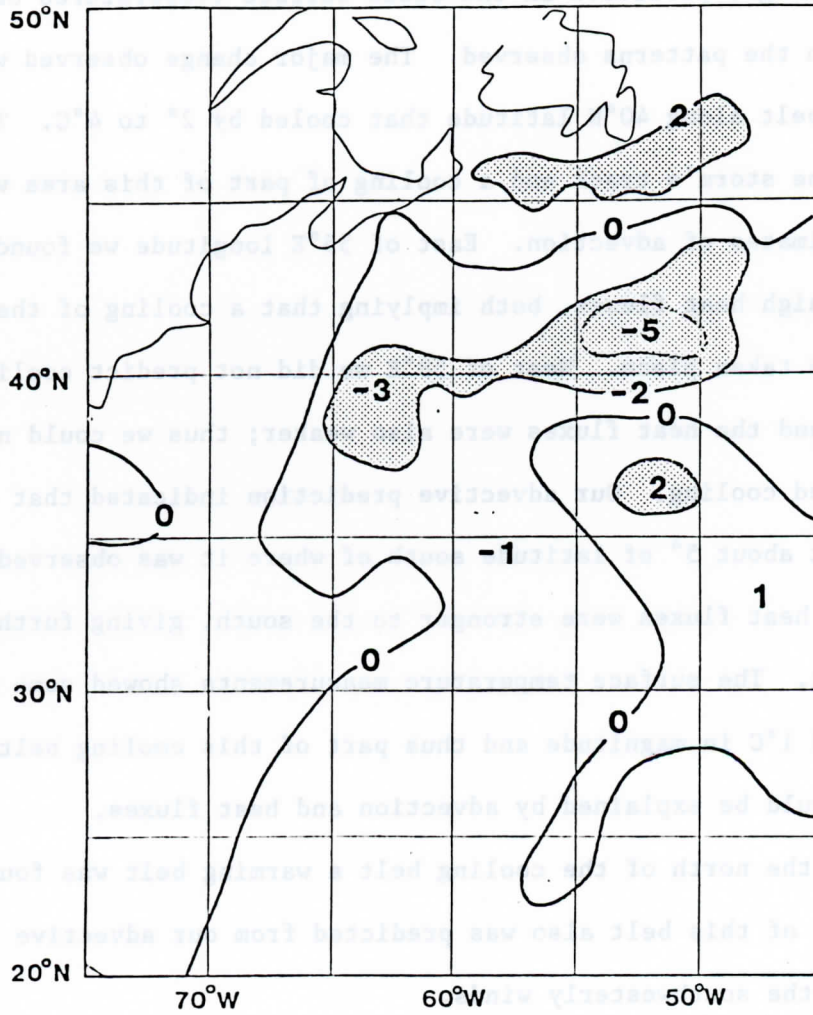
49

Fig. 24. An estimation of the surface temperature changes
caused by the advection of wind driven currents.

The results of applying (3), (7), and (6) to the temperature and wind analyses (Figs. 13 and 20) are shown in Fig. 24. This is a prediction of the surface temperature changes over a period of two days.

4.5 Evaluation

The changes predicted in the ocean surface temperatures only partially agreed with the patterns observed. The major change observed was the east-west belt along 40°N latitude that cooled by 2° to 4°C. This belt was north of the storm's track and a cooling of part of this area was predicted by our estimates of advection. East of 55°E longitude we found northerly winds and high heat fluxes, both implying that a cooling of the ocean should have taken place. West of 58°E we did not predict cooling by advection and the heat fluxes were also weaker; thus we could not explain the observed cooling. Our advective prediction indicated that cooling was possible at about 5° of latitude south of where it was observed, along 35°N. The heat fluxes were stronger to the south, giving further evidence for cooling. The surface temperature measurements showed some cooling at 35°N around 1°C in magnitude and thus part of this cooling belt occurred where it could be explained by advection and heat fluxes.

Farther to the north of the cooling belt a warming belt was found along 46°N. Part of this belt also was predicted from our advective calculations because of the southwesterly winds.

At 36°N and 51°E 2°C of warming were found. This feature was not predicted by our analysis. Wind data from this area was sparse mainly because of cirrus cloud and SEASAT orbital coverage as previously mentioned. Thus, we may not have properly predicted the surface currents in the area.

51

For part of the area the estimated wind driven currents were in the opposite direction from the prevailing currents. Along the coast of North America we found southwesterly winds and thus predicted southwesterly currents from 37°N to Nova Scotia. This is where the northerly Labrador current has been commonly found and wind currents are not expected. We do not fully know the extent to which the Labrador current caused the temperature changes.

The winds also oppose the expected direction over part of the Gulf Stream. A westerly current along 37°N latitude has generally been found, while our analysis found easterly winds at the same latitude.

To the south of the storm's track no major temperature changes were found. The advective estimates also did not predict any changes. However, the heat fluxes were very strong west of 65°W, which implied that some cooling should have taken place.

The heat fluxes, however, may have been more important to the convective clouds in the storm than the energy budget of the ocean. From the strong southwesterly winds that entered the storm from the south, it is apparent that the convective clouds obtained most of their energy from the air to the south of the storm. This flow picked up a large quantity of heat and moisture near the storm as shown by the heat flux analysis. According to our wind patterns, the cold air to the north of the storm did not feed directly into the storm. While the backside of the cold surge from the previous storm curved toward Hope, the air did not appear to substantially enter Hope from the north.

In summary, the study was not extremely successful from the standpoint of predicting surface temperature changes. Possibly the chief difficulty was reliance on ship observations for surface temperatures. However, it

provided an important learning exercise in combining data from various sources. The symbiotic relationship among cloud motions, ship observations, and scatterometer winds is best illustrated in the final figure (Fig. 25).

5.   Reprise

This report has covered much material. We would now like to present to the reader our conclusions which are based both on the studies presented above, and especially on our experience.

- Cloud motions can be used to de-alias scatterometer winds -- if it is done thoughtfully with due regard to cloud type, orography, and air-sea temperature difference climatology.

- Because of swath width and coverage characteristics the SEASAT scatterometer does not constitute a complete observing system exploiting its 100 or 50 km resolution. It could, preferably, be flown on a multi-satellite system, or at least as a valuable adjunct to other observing systems like ships and cloud motions.

- After alias removal, the flow patterns revealed by the scatterometer seemed consistent with the meteorological phenomena seen in the geostationary movie loops.

We refer the reader to the recent study by Schroeder et al. (1983) which suggests that it is feasible to build a scatterometer with sufficient skill to build a self-initiating iterative de-aliasing scheme. This motivates our final point.

Winds at cloud level and winds near the surface may give us valuable information on the state of the intervening atmosphere. Possibly the speed and direction differences across this lowest 100 mb which are closely

53

Fig. 25.   Contributions of ship, cloud, and scatterometer wind data on 15 September 1978.   In part a (above), scatterometer observations are shown as vectors, ship observations as flags.   In part b (following page), the flags are cloud motion observations.
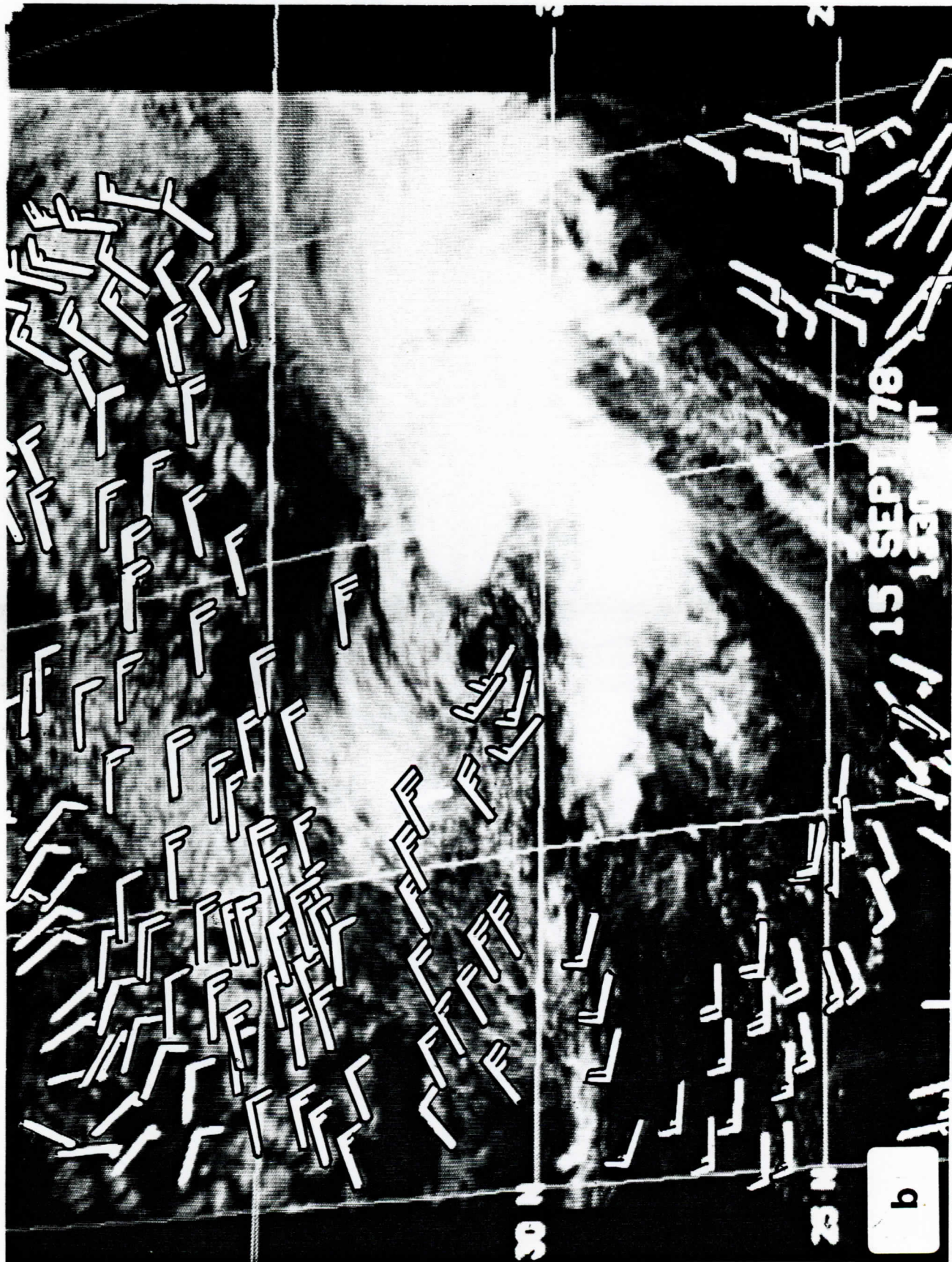
54

Figure 25 Continued

related to ocean–atmosphere momentum transport can be used as one index of stability and transports of heat and moisture. In our case study, we used all the winds as surface winds. With better space-time coverage from a scatterometer, two levels can be considered.

8/SEASAT/01

References

Agee, E.M., T.S. Chen, and K.E. Dowell, 1973: A review of mesoscale cellular convection. _Bull. Amer. Meteor. Soc._, 54, 1004-1012.

Cox, C. and W. Munk, 1954: Measurements of the roughness of the sea surface from photographs of the sun's glitter. _J. Opt. Soc. Amer._, 44, 838-850.

Dunkel, M., L. Hasse, L. Krügermeyer, D. Schriever, and J. Wucknitz, 1974: Turbulent fluxes of momentum, heat, and water vapor in the atmospheric surfce layer at sea during ATEX. _Boundary-Layer Met._, 6, 81-106.

Francey, R.J., and J.R. Garratt, 1978: Eddy flux measurements over the ocean and related transfer coefficients. _Boundary-Layer Met._, 14, 153-166.

Grantham, W.L, E.M. Bracalente, W.L. Jones, and J.W. Johnson, 1977: The SEASAT-A satellite scatterometer. _IEEE J. Oceanic Eng._, OE-2, 200-206.

Grantham, W.L., E.M. Bracalente, C.L. Britt, Sr., F.J. Wentz, W.L. Jones, and L.C. Schroeder, 1982: Performance evaluation of an operational spaceborne scatterometer. _IEEE Trans. Geosci. and Rem. Sens._, GE-20, 250-254.

Hayden, C.M., 1979: Remote soundings of temperature and moisture, in _Quantitative Meteorological Data from Satellites_, J. S. Winston, Ed., WMO Tech. Note No. 166, World Meteorological Organization, Geneva.

Hicks, B.B., 1975: A procedure for formulation of bulk transfer coefficients over water. _Boundary-Layer Met._, 8, 515-524.

Hubert, L.F., 1979: Wind derivation by geostationary satellites, in _Quantitative Meteorological Data from Satellites_, J.S. Winston, Ed., WMO Tech. Note No. 166, World Meteorological Organization, Geneva.

Johnson, J.W., L.A. Williams, Jr., E.M. Bracalente, F.B. Beck, and
W.L. Grantham, 1980: SEASAT-A scatterometer instrument evaluation.
IEEE J. Oceanic Eng., OE-5, 138-144.

Kirwan, A.D., G. McNally, S. Pazan, and R. Wert, 1979: Analysis of surface
current response to wind. J. Physical Ocean., 9, 401-412.

Mosher, F.R., 1979: Cloud drift winds from geostationary satellites. Atmos.
Techn., NCAR, No. 10, 53-60.

Pollard, R.T., 1977: Observations and models of the structure of the upper
ocean. Modelling and Prediction of the Upper Layers of the Oceans,
E.B. Krauss, Ed, Pergamon Press, New York, 325 pp.

Pond, S., D.B. Fissel, and C.A. Paulson, 1974: A note on bulk aerodynamic
coefficients for sensible heat and moisture fluxes. Boundary-Layer
Met., 6, 333-339.

Schroeder, L.C., W.L. Grantham, E.M. Bracalente, C.L. Britt,
K.S. Shanmugam, F.J. Wentz, D.P. Wylie, and B.B. Hinton, 1983: A study
of removal of ambiguous wind direction results for a Ku-band
scatterometer wind sensor using measurements at three different
azimuth angles, in International Geoscience and Remote Sensing
Symposium 1983 Digest, Fresno, CA, 31 August-2 September 1983.

Smith, S.D., 1980: Wind stress and heat flux over the ocean in gale force
winds. J. Phy. Ocean., 10, 709-726.

Suomi, V.E., R. Fox, S.S. Limaye, and W.L. Smith, 1983: McIDAS III: A
modern interactive data access and analysis system. J. Clim. and Appl.
Meteor., 22 (in press).

Wu, J., 1980: Wind-stress coefficients over sea surface near neutral
conditions -- a revisit. J. Phy. Ocean., 10, 727-740.

Wylie, D.P., and B.B. Hinton, 1981: The feasibility of estimating oceanic wind stress for the summer MONEX using cloud motion and ship data. Boundary-Layer Met., 21, 357-367.

Wylie, D.P., B.B. Hinton, and K.M. Millett, 1981: A comparison of three satellite based methods for estimating surface winds over oceans. J. Appl. Met., 20, 439-449.

59

Appendix A

Reprinted from JOURNAL OF APPLIED METEOROLOGY, Vol. 20, No. 4, April 1981
American Meteorological Society
Printed in U. S. A.

A Comparison of Three Satellite-Based Methods for Estimating Surface Winds over Oceans

DONALD P. WYLIE, BARRY B. HINTON AND KELLIE M. MILLETT[1]

Space Science and Engineering Center, University of Wisconsin-Madison, Madison, WI 53706

ABSTRACT

The feasibility of using satellites for providing surface winds or wind stress data was explored. Three popular methods were compared using nearly colocated data to assess the accuracies of each and the coverage that each could provide. The three methods tested were 1) the use of the sun glitter reflection seen on visible images of the ocean surface; 2) the use of active microwave sensors (flown on SEASAT) which reflect microwaves off the ocean surface; and 3) the use of cloud motions as indicators of the surface winds.

Close agreement in wind speed estimates was found among the three methods. The biases were <0.6 m s^{-1} for comparisons between comparable methods of estimating surface winds (1 and 2). Cloud motion comparisons to the other methods exhibited biases of <3.0 m s^{-1}. Individual point-by-point comparisons between wind measurements had an average scatter of 2.0 m s^{-1} (rms) or less after the mean biases were removed. Atmospheric variability caused as many of the differences as the instrumental errors indicating that meaningful wind information could be obtained from all three methods.

Very detailed spacial coverage was obtained with the sun-glitter method for wind speeds. However, the coverage was restricted to a narrow band 5° of latitude wide in the tropics. SEASAT also provided good coverage for two swaths (4° longitude wide) on each side of the satellite's orbit. Gaps between the swaths and orbits (polar non-synchronous orbits) were left unsampled. Both methods required external data on the wind directions which were obtained from cloud motions. The cloud motions provided coverage over larger areas than the other two methods because of the abundance of low-level cumuli.

The following pages contain material extracted from the original article, to which the reader is referred for details.

All three methods were compared in two geographical areas: the eastern Pacific off the coast of Columbia, South America, and the Atlantic northeast of Brazil. Both areas were in the tropics because of the restrictions of the sun glitter method (see Table 2).

TABLE 2. The basic characteristics of the areas used for the comparisons.

	Pacific	Atlantic
Bounds		
Latitude	2°S–6°N	4–19°N
Longitude	80–99°W	39–55°W
Range of cloud-motion speeds	3–10 m s^{-1}	3–15 m s^{-1}
Range of surface wind speeds (glitter method)	2–8 m s^{-1}	3–10 m s^{-1}
Range of air-sea temperature difference (ship reports)	−1 to −5°C	−8 to +7°C

Two days were studied in each area. One SEASAT oribt per day was chosen for the comparisons. All SEASAT orbits used passed through the areas within 3 h of the time of passage of the sun glitter. GOES images also were selected to coincide with the passage of the sun glitter.

In the Pacific comparisons with two ship observations indicated that the atmospheric boundary layer was unstable with reported air temperatures of 1–5°C colder than the water on both days. The exact magnitude of the temperature difference was difficult to assess because a 5°C air-sea temperature difference is not realistic over the ocean. However, consistently unstable conditions for this area were found in the climatological analysis of Hastenrath and Lamb (1977).[4]

The wind estimates were grouped into pairs for the comparisons. All cloud vectors, SEASAT vectors, or glitter vectors within 1° latitude and longitude were averaged. One sun-glitter estimate was made in the area of each SEASAT vector or cloud.

TABLE 3. Average differences between colocated wind-vector pairs (m s^{-1}) within 1° of latitude or longitude of each other. The number of paired vectors is given in parentheses.

Date	Loca-tion	Clouds* – Sun glitter	SEASAT – Sun glitter	Clouds* – SEASAT
16 Jul 78	Atlantic	3.0 (12)	0.6 (13)	0.8 (148)
17 Jul 78	Atlantic	2.2 (38)	−0.2 (33)	2.2 (116)
13 Sep 78	Pacific	−0.9 (17)	0.3 (24)	−0.8 (43)
16 Sep 78	Pacific	0.8 (12)	−0.2 (11)	0.5 (8)
Both Atlantic				9.7° (264)
Both Pacific				−3.3° (51)

* Corrections for wind shear in the boundary layer have not been applied.

TABLE 4. The rms deviations (m s^{-1}) of the vector pair differences, i.e., the scatter of one measurement about the other using colocated vector pairs.

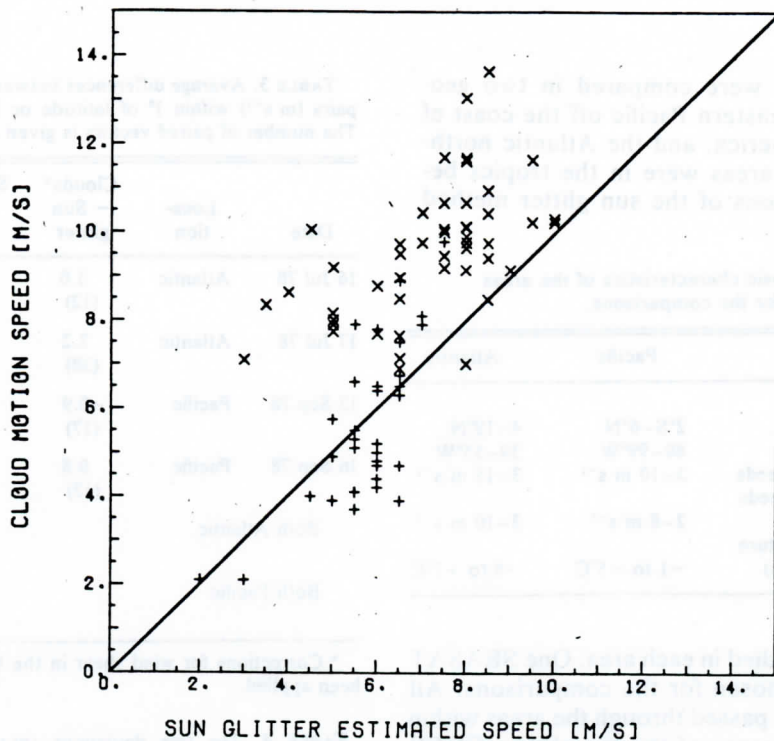| Date	Clouds – Sun glitter	SEASAT – Sun glitter	Clouds – SEASAT
16 Jul 78	±1.4	±0.7	±1.9
17 Jul 78	1.5	1.2	1.2
13 Sep 78	0.6	0.9	0.9
16 Sep 78	1.3	1.3	1.3
Atlantic			15.8°
Pacific			14.2°

A2

SUN GLITTER VS CLOUDS

FIG. 4. The comparison of cloud motions to the sun glitter surface wind estimates:
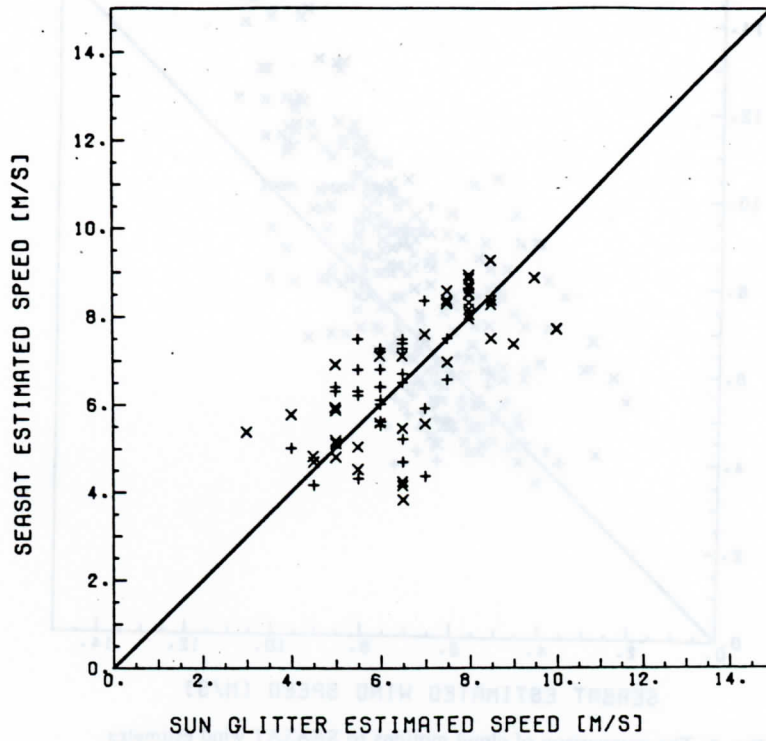(+) Pacific area, (×) Atlantic area.

A3

FIG. 5. The comparison of SEASAT wind estimates to the sun glitter wind estimates: (+) Pacific, (×) Atlantic.
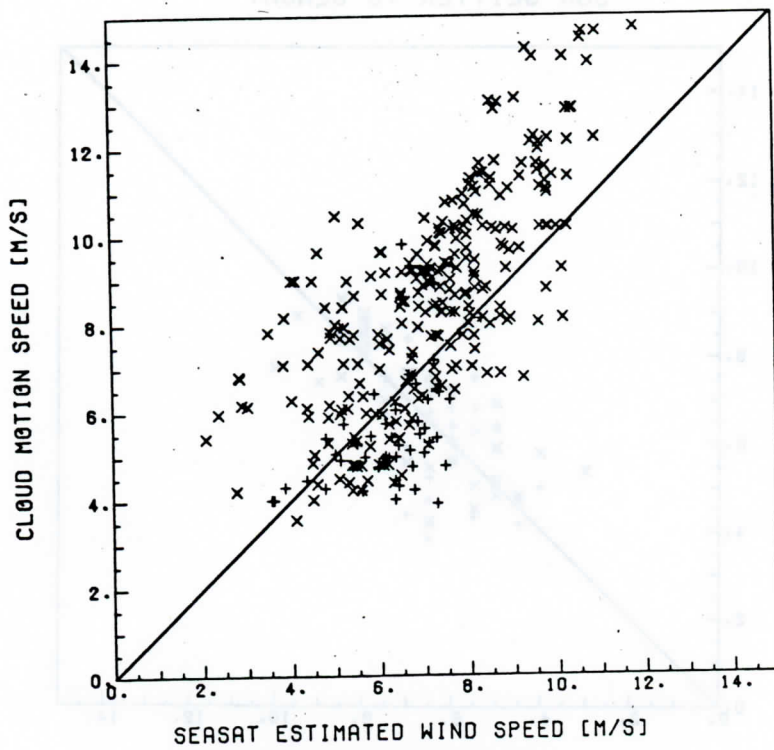
A4

SEASAT VS CLOUDS

FIG. 6. The comparison of cloud motions to SEASAT wind estimates:
(+) Pacific area, (×) Atlantic area.

A5